A visual atlas of meiotic protein dynamics in living fission yeast

Wilber Escorcia*[1,2], Vishnu P. Tripathi*[1], Ji-Ping Yuan[1], and Susan L. Forsburg[1, #]

1. University of Southern California, Molecular and Computational Biology Program
2. University of Southern California, Leonard Davis School of Gerontology

Corresponding author: forsburg@usc.edu

* Equal contribution

Running Title: A Meiosis Atlas

Key Words: Meiosis, Histone, Cohesin, Microtubule, Spindle Assembly Checkpoints, PCNA

ORCID:

Susan L. Forsburg: 0000-0002-4895-8598

Vishnu P. Tripathi: 0000-0002-6137-8547

Wilber Escorcia: 0000-0002-2141-0581

Summary

Meiosis is an important process for sexually reproducing organisms. Unique dynamics of recombination and chromosome segregation are required for this differentiation process. Fission yeast is an excellent model to study meiotic progression and chromosome dynamics. In this report, using fluorescently tagged proteins and live-cell microscopy we present meiotic signposts that define dynamic behavior of proteins during meiotic DNA synthesis, nuclear fusion, chromosome alignment, genetic recombination, metaphase, and meiosis.

Abstract

Meiosis is a carefully choreographed dynamic process that re-purposes proteins from somatic/vegetative cell division, as well as meiosis-specific factors, to carry out the differentiation and recombination pathway common to sexually reproducing eukaryotes. Studies of individual proteins from a variety of different experimental protocols can make it difficult to compare details between them. Using a consistent protocol in otherwise wild type fission yeast cells, this report provides an atlas of dynamic protein behavior of representative proteins at different stages during normal zygotic meiosis in fission yeast. This establishes common landmarks to facilitate comparison of different proteins and shows that initiation of S phase likely occurs prior to nuclear fusion/karyogamy.

Introduction

Meiosis is a conserved cell differentiation pathway found in sexually reproducing eukaryotes. It is characterized by one round of DNA synthesis, followed by two nuclear divisions, resulting in haploid gametes (reviewed in (Zickler and Kleckner, 1999); (Cavalier-smith, 2002; Hochwagen, 2008; Ohkura, 2015)). In most organisms, the divisions are preceded by programmed double strand breaks (DSB) followed by homologous recombination (HR) that facilitates separation of the homologous chromosomes during reductional meiosis I division (reviewed in (Gray and Cohen, 2016)). The equational meiosis II division separates sister chromatids and more closely resembles mitosis in somatic or vegetative cells but is unusual in that it does not follow a period of DNA synthesis (reviewed in (Ohkura, 2015)).

A variety of meiosis-specific genes are recruited to facilitate these specialized events. These include additional recombination proteins, components of the synaptonemal complex or linear elements between chromosome homologues, proteins that contribute to kinetochore mono-orientation, and meiosis-only cohesin proteins that link sister chromatids together. These specialists modify the basic architecture of cell division particularly to facilitate the meiosis-specific chromosome recombination and the MI division mechanisms (Hunter, 2015; Lam and Keeney, 2015; Zickler and Kleckner,

2015). The yeast *Schizosaccharomyces pombe* offers an excellent model system to study the process of meiosis. Normally haploid cells can be induced to conjugate with cells of the opposite mating type in conditions of nutrient limitation, forming transient zygotes. The initial landmark event following karyogamy is the formation of a telomere-led chromosome bouquet, which migrates rapidly back and forth in the length of the cell in a dynein-led movement called horse-tailing (HT) (Ding et al., 1998; Yamamoto et al., 1999). Meiotic S (meiS) phase and recombination occur during horse-tailing, which is followed by the MI and MII divisions (reviewed in (Davis and Smith, 2001; Mizuguchi et al., 2015; Yamashita et al., 2017). Genetic tools have been deployed to identify and characterize proteins that function throughout these different phases.

The advent of green fluorescent protein (GFP) and related colorful fluorescent tags has allowed the analysis of protein dynamics in living cells and these have been widely used in studies of fission yeast meiosis. However, variation in protocols and conditions make it challenging to compare the dynamics of proteins in the various stages of meiosis in different publications. In particular, many studies employ a temperature sensitive pat1 mutant to drive a synchronous meiosis, even from haploids, which disrupts aspects of meiosis (e.g., (Bähler et al., 1991; Iino and Yamamoto, 1985a; Yamamoto and Hiraoka, 2003). In this report, we examine protein dynamics in meiosis using consistent strains, growth conditions and a standardized imaging protocol (Escorcia et al., 2019; Green et al., 2015). This allows us to generate an atlas of meiotic protein behavior that will be useful to a variety of investigators studying this dynamic process.

Results

Rationale We used a uniform growth strategy to induce mating and meiosis between cells of opposite mating types, followed by imaging of cells on agar pads (see Methods (Escorcia and Forsburg, 2017; Escorcia et al., 2019)). Importantly, aside from the tagged genes, the strains are normal haploids that were induced to mate, followed by zygotic meiosis. Reasonable synchrony was achieved solely by using appropriate growth conditions, and we did not employ any mutations such as *pat1-ts* which can

induce meiotic abnormalities (e.g., (Bähler et al., 1991; Yamamoto and Hiraoka, 2003)). Thus, our strategy recapitulates as much as possible a “normal” fission yeast meiosis.

Nuclear dynamics establish a reference

Hht1 and Hhf1 are the H3-H4 histone pairs used for nucleosome packaging of DNA in fission yeast (Choe et al., 1985; Takayama and Takahashi, 2007). Because of its role in nuclear organization, Hht1 is used with fluorescent tags to mark the nuclear mass during mitotic and meiotic processes (Escorcia and Forsburg, 2017; Sabatinos et al., 2015; Tomita et al., 2013). We employed cells carrying either Hht1-mRFP or Hht1-GFP and followed meiotic progression using live-cell imaging. We began our observations during the phase following initial mating but prior to karyogamy, which we term the pre-fusion stage (PF). At this stage, Hht1 signal is pan-nuclear and shows no drastic movements or changes in shape (FS-HT: -10 min) (**Fig. 1A, Fig. S1A, B**). Nuclear fusion (FS) occurs and is characterized by nuclear bridging, where genetic material is combined (FS-HT: 0 min) (**Fig. 1A, Fig. S1A, B**). After completion of karyogamy, mixing takes place and the nuclear size doubles in the zygote relative to haploid, pre-fusion cells (FS-HT: -10 to 10 min) (**Fig. 1A, Fig. S1A, B**). This period of nuclear fusion lasts for about 14 minutes (mean timing= 14.1’ ± 2.6’) before the nuclear mass undergoes repeated oscillations for approximately 215 minutes (215.5’ ± 15.8’) in the horse-tailing stage (HT) (**Fig. 1B**). The horse-tailing phase marks the period in which meiotic chromosome recombination takes place (Cooper et al., 1998; Hiraoka et al., 2000).

When horse-tailing concludes, vigorous oscillation ceases, and the nuclear size starts to contract, with moderate to low nuclear movement (HT-MTI: -50 to -30 min) (**Fig. 1 A**). This transition phase of nuclear reconfiguration lasts for approximately 20 minutes (23.2’ ± 1.7’) followed by 8 minutes (8.4’ ± 1.8’) of metaphase I (MTI) where maximal nuclear compaction occurs and Hht1-mRFP signal intensifies (HT-MTI: -20’ to 0’) (**Fig. 1 A-C, Fig. S1A, C, D**). The nucleus in meiosis I (MI) splits into two nuclear masses of roughly equal size (MTI-MI: 10’) (**Fig. 1 A, Fig. S1A**) that contain segregated sets of homologous chromosomes (Hauf et al., 2007; Hirose et al., 2011; Yokobayashi and Watanabe, 2005). The transition of metaphase I to meiosis I lasts for approximately 10 minutes (10.3’ ± 0.5’) whereas the average duration of meiosis I to meiosis II is

approximately 50 minutes (53.2’ ± 2.2’) (**Fig. 1B**). During metaphase II (MTII), homologs continue to move toward opposite ends of the zygote. Final separation of the two nuclear masses into four daughter nuclei marks the completion of meiosis II (MII) (MTI-MI: 60-70) (**Fig. 1 A, Fig. S1A**). At this stage, sister chromatid sets completely segregate and are readied for packaging into spores in the gamete-maturation phase that follows meiosis II (Hauf et al., 2007; Hirose et al., 2011; Yokobayashi and Watanabe, 2005).

S phase markers PCNA and Tos4

PCNA (SpPcn1) plays major roles in DNA replication, repair and translesion synthesis (revived in (Boehm et al., 2016)). A processivity factor, it interacts with both DNA Polymerase δ and ε (Arroyo et al., 1996; reviewed in (Choe and Moldovan, 2017)). In *S pombe,* GFP tagged Pcn1 has been used in DNA replication studies ((Meister et al., 2007; Ruan et al., 2015a). To monitor meiotic S phase dynamics, we used EGFP-Pcn1 (Meister et al., 2007). Consistent with data from vegetative cells (Meister et al., 2007), we observed discrete EGFP-Pcn1 foci. These initially appeared throughout the nucleus at the pre-fusion stage (FS-HT: -10’) which lasted for about 10 minutes (11.1 ± 1.1’) (**Fig. 2A, B**). At karyogamy, when the two parent nuclei fused, the EGFP-Pcn1 foci remained pan nuclear and signal intensity went up and reached to the maximum (FS-HT: 0’) (**Fig. 2C**). As cells moved from karyogamy to the horse-tailing stage, pan nuclear, punctate foci diffused and large replication foci formed at one end of the nucleus which later converted into fewer and smaller foci, again localized in one edge of the nucleus (FS-HT: 0’-30’) (**Fig. 2A**). Before Pcn1-GFP signal became diffusely distributed, this replication patterns of PCNA, during karyogamy and early horse-tailing stage last for about 49 minutes (48.9’ ± 8.1’) (**Fig. 2B**). Notably, horse-tailing continues for another 160-180 minutes but Pcn1 signal remains diffused, suggesting the conclusion of S phase.

Fission yeast Tos4 is a nonessential transcription factor that accumulates during early S-phase in the nucleus (Bastos de Oliveira FM et al., 2012; Kiang et al., 2009; Kim et al., 2020; Shen and Forsburg, 2019) Tos4 contains a fork-head associated (FHA) domain and is regulated by the G1/S transcription factors SBF (Swi4-Swi6 cell cycle box

binding factor) (Horak et al., 2002; Huang and Elledge, 2000). We used fluorescently tagged Tos4-GFP to examine its behavior in meiosis (Kim et al., 2020; Shen and Forsburg, 2019). The expression of bright pan-nuclear Tos4-GFP signal was first observed during the pre-fusion stage, lasting for about 11 minutes (11.3' ± 1.9') (FS-HT: -10 min) (**Fig. 2D, E**). The signal intensity of Tos4-GFP foci increases as cells undergo karyogamy (FS-HT: 0 min) (**Fig. 2F**). The pan-nuclear Tos4-GFP signal gradually disappears as cells spend about 25-30 minutes in horse-tailing (FS-HT: 0 to 30 min) (**Fig. 2D, F**). The duration of pan-nuclear Tos4 signal from fusion to early horse-tailing is observed for about 40 minutes (41.3' ± 3.5') (**Fig. 2E**). Notably, the dynamics and timing of Tos4-GFP accumulation in the nucleus is similar to the EGFP-Pcn1, although EGFP-Pcn1 replication foci last approximately 8 min longer. This suggests that Tos4-GFP is an early meiotic S phase marker with similar dynamics to vegetative S phase (Kim et al., 2020).

Cohesin and pairing proteins

Rec8 is the alpha-kleisin subunit of the meiotic cohesin complex in fission yeast (Ding et al., 2006; Ding et al., 2016; Watanabe and Nurse, 1999; Watanabe et al., 2001). Following meiotic DNA synthesis, it keeps sister chromatids cohered at the centromere until just before meiosis II, when it is degraded to allow sister chromatid separation (Ishiguro et al., 2010; Kitajima et al., 2004; Kitajima et al., 2006; Riedel et al., 2006). We examined the meiotic nuclear dynamics of cells in which Rec8 is tagged with green fluorescent protein (Rec8-GFP). Rec8-GFP signal is observed in cells prior to karyogamy (FS-HT: -10 to 0) (**Fig. S2A-C**). This signal is dispersed throughout the nucleus and during nuclear fusion, horse-tailing, and metaphase I (FS-HT: -10 to 60 min; HT-MTI: -60 to 0 min) (**Fig. S2A-C, Fig. 3A, B**). Approximately, within the first 15 minutes (15.4' ± 2.2') of meiosis I, Rec8-GFP signal intensity decreases drastically (MTI-MI: 0 to 20) until it becomes a focus in each nucleus during meiosis I and metaphase II (MI-MTII: 10'-50') (**Fig. 3A-E**). Just before cells enter meiosis II, the Rec8-GFP focus in each nucleus disappears (MTII-MII: 50'-70') (**Fig. 3A**). Complete loss of Rec8-GFP signal precedes the final equational division of meiosis II and it takes about 35 minutes (35.7' ± 2.9') after meiosis I to complete (MTI-MI: 10-50 min) (**Fig. 3D**).

Rec27 and Rec10 are part of the linear element (LinE) proteins that bind along the axes of homologous chromosomes to regulate chromosome pairing, programmed double strand breaks (DSB), and genetic recombination (Davis et al., 2008; Ellermeier and Smith, 2005; Phadnis et al., 2015; Sakuno and Watanabe, 2015). We followed cells in which Rec27 is fluorescently tagged (Rec27-GFP). We observe Rec27-GFP pan-nuclear signal during the period preceding nuclear fusion (**Fig. S4**). The signal continues until late horse-tailing stage (HT-MTI: -40') (**Fig. S4**). However, the pan-nuclear dispersed signal migrates into discrete puncta that gradually decrease in intensity and number before metaphase I (HT-MTI: -50 to -30 min) (**Fig. S3A, B, E**). The disappearance of LinE foci happens about 19 minutes (19.1' ± 3.2') prior to the onset of metaphase I (**Fig. S3 D**). We did not observe Rec27-GFP signal in metaphase I or following meiosis I and II (MTI-MI: -20 to 70 min) (**Fig. S3A,B**).

Sgo1 (*shugoshin)* along with phosphatase protein 2A (PP2A) helps to protect Rec8 from proteolytic degradation at the centromere prior to meiosis I (Ishiguro et al., 2010; Kitajima et al., 2004; Riedel et al., 2006). We observed meiosis in cells carrying Sgo1 fluorescently tagged with GFP (Sgo1-GFP). Sgo1-GFP signal emerges when nuclear oscillation slows down in horse-tailing and remains visible for 50-55 minutes before disappearing during the metaphase I to meiosis I transition (HT-MTI: -60 to 0 min) (**Fig. S5A, B, E**). The discrete Sgo1-GFP foci disappears in about 11 minutes (11.4' ± 1.1') of metaphase I to meiosis I transition (**Fig. S5D**). During meiotic divisions, only background signal is observed (MTI-MI: 0 to 70 min) (**Fig. S5A, E**).

Moa1 (monopolin) is required to establish monopolar attachment of sister chromatids during meiosis I. It associates with Rec8 at the centromere and helps to stabilize Sgo1, thereby ensuring protection of centromeric cohesion, which is crucial for separation of homologous chromosomes (Galander et al., 2019; Hirose et al., 2011; Sakuno et al., 2009; Yokobayashi and Watanabe, 2005). Similar to Sgo1-GFP, we found that Moa1-GFP foci are observed for about 48 minutes (48.6 ± 3') previous to and during metaphase I (MTI-MI: -60 to 0 min) (**Fig. 4A-E**). These foci are first dispersed around the nucleus and later cluster together at discrete spots in opposite directions as the nuclear mass condenses in preparation for homolog separation in meiosis I (HT-

MTI: -10 to 0 min) (**Fig. 4A-C**). During early MI, we observe Moa1 at the poles of the spindle in addition to spots in the center, likely corresponding to the centromere. Within about first 14 minutes (14' ± 2') of metaphase I to meiosis I transition, we observe a complete loss of Moa1 foci (**Fig. 4D**). We did not see any signal in later stages of metaphase II and meiosis II (**Fig. 4A, B**).

Recombination and Repair

Rad11 (Ssb1) is the fission yeast orthologue of replication protein A (RPA), which binds to single stranded DNA (ssDNA) resulting from replisome progression in DNA synthesis and processing of DSB during DNA repair and homologous recombination (Escorcia and Forsburg, 2017; Mastro and Forsburg, 2014; Parker et al., 1997; Sabatinos et al., 2012). We examined cells with fluorescently marked RPA (Rad11-CFP) to observe signal dynamics previous to and during the meiotic nuclear divisions. Rad11-CFP signal is pan-nuclear while meiotic DNA synthesis (data not shown) and recombination take place (HT-MTI: -60' to -30') (**Fig. 5A, C**). During horse tailing, we observe foci that increase in intensity as the nucleus becomes condensed before and during metaphase I (MTI-MI: -60 to 0 min) (**Fig. S6D**). The end of discrete Rad11 foci signal occurs about 21 minutes (21' ± 2.3') prior to the onset of metaphase I (**Fig. S6B)**. After meiosis I, for next 53 minutes (53.4' ± 1.8'), Rad11-CFP dissipates along the newly formed nuclei until signal is near background levels by meiosis II (MTI-MI: 0 to 70 min) (**Fig. 5A, Fig. S6D).**

Rad52 acts with Rad11 and Rad51 to regulate recombination, which facilitates reductional division of the homologous chromosomes in meiosis I (Murayama et al., 2013; Muris et al., 1997; Octobre et al., 2008; van den Bosch et al., 2001). There are discrete punctate foci of Rad52-YFP during the late stage of horse-tailing (MTI-MI: -50 to -20 min) which decrease in intensity and diffuse as the cells enter metaphase I (MTI-MI: 0 to 70 min) (**Figs. 5B, C, Fig. S6A, E**). This stage lasts for about 15 minutes (15' ± 3') prior to metaphase I (**Fig. S6C**). In strains also expressing Rad11-CFP, we observed a signal colocalization with Rad52-YFP prior to and during metaphase I (MTI-MI: -50 to 0 min) (**Fig. 5C, Fig. S6A**). Both Rad52 and RPA puncta are resolved by the time cells

proceed through meiosis I division. We observed a diffuse nuclear Rad52 signal for about 55 minutes (55’ ± 1’) after meiosis I until finally it disappears **(Fig. S6D, E)**.

Spindle and spindle checkpoint dynamics

Atb2, a nonessential component of α-tubulin, is a constituent of cytoplasmic microtubule organization and is actively involved in establishment and maintenance of cell polarity and cell shape (Adachi et al., 1986; Radcliffe et al., 1998). Previously, several studies have shown microtubule dynamics covering specific meiotic events e.g., karyogamy to prophase, or prophase to meiosis II (Ding et al., 1998; Fennell et al., 2015; Okamoto et al., 2012; Yamamoto et al., 2008). Here we captured microtubule dynamics throughout an unperturbed zygotic meiosis, beginning prior to karyogamy. We employed heterothallic strains containing mCherry tagged atb2 (Atb2-mCherry) (Yamagishi et al., 2008) and GFP tagged hht1 and imaged meiotic progression from pre-fusion to meiosis II. We used the nuclear dynamics of Hht1 as the landmarks for pre-fusion, karyogamy, horse-tailing, metaphase I, meiosis I and II events. In the pre-fusion stage, we observed a bundle of microtubules extending all across the cell which stayed for 15 minutes (FS-HT: -220 to -200) **(Fig. S7A)**. During that stage, hht1-GFP appeared diffused. As cells enter karyogamy, the bundle of microtubules moves and finally converges to form a X shaped structure, bringing the spindle pole in the center and two parent nuclei closer. Karyogamy lasted for about 15 minutes (FS-HT: -200’ to -180’) (**Fig. S7B)**. Zygote formation and nuclear oscillation in the horse-tailing stage lasted for 150-160 min (FS-HT: -180’ to -30’). During horse-tailing, microtubules oscillate across the cell, consistent with prior reports (Ding et al., 1998; Fennell et al., 2015) (HT-MTI: -60 to -30) **(Fig. 6A, B, Fig. S7A)**. As cells approach the end of horse-tailing, we observed a continuous spindle depolymerization represented by reduction in microtubule length and signal intensity (**Fig. 6A, B, D)**. This spindle depolymerization, during the late horse-tailing stage, lasts for about 39 minutes (39’ ± 4.5’) (**Fig. S7B)**. A discrete Atb2 focus reappears 12 minutes (12’ ± 1.4’) prior to the metaphase I, representing prophase I (HT-MTI: -60’ to -20’) (**Fig. 6A, B, Fig. S7B)**. The prophase I stage is marked by gradual spindle elongation with increase in the intensity and the length. Maximum signal intensity and slight increase in constant spindle lengths

represents the end of the metaphase I which lasts 12 minutes (12.3’ ± 1.5’) (HT-MTI: -20’ to 0’) **(Fig. 6A, D, Fig. S7B)**). During anaphase I (meiosis I), the meiotic spindle, elongates outwards and reaches the cell tip. This elongation occurs as the chromosomes separate in two daughter nuclei and it lasts for about 10 minutes (10.9’ ± 1’) (MTI-MI: 0’ to 20’) (**Fig. 6A, D, Fig. S7B)**. The completion of meiosis I is followed by loss of signal associated with microtubule depolymerization and spindle breakdown (MI: 20’ to 40’) (**Fig. 6A, B, Fig. S7B)**. The duration of Meiosis I is about 34 minutes including approximately 11 minutes (10.9’ ± 1’) of anaphase 1 with extended spindle elongation, and 23 minutes (22.9’ ± 1.8’) of an interval with loss of signal (**Fig. S7B)**. During prophase II, Atb2-mCherry signal reappears as a single focus followed by an extension of microtubules leading to metaphase II and anaphase II. Microtubule dynamics in meiosis II were similar to meiosis I (**Fig. 6A, D)**. Finally, at the end of meiosis II the nuclear microtubule signals disappear again. The duration of metaphase II lasted approximately 12 minutes (12.3’ ± 1.5’) while the anaphase II lasted for about 14 minutes (14.6’ ± 1.8’) (**Fig. S7B)**. The spindle length and signal intensity in meiosis I and II are proportional to the respective nuclear mass (hht1-GFP) (**Fig. 6D)**. Completion of meiosis II is represented by completely separated four daughter nuclei and depolymerization of the microtubule (MI-MII: 40’ to 70’) (**Fig. 6A, B)**.

Aurora-B like kinase (*Sp*Ark1) is a serine/ threonine kinase and a component of chromosome passenger complex which ensures phosphorylation of substrates involved during chromosome condensation activation of spindle assembly checkpoints and correction of erroneous kinetochore-microtubule attachments (Carmena et al., 2012; Kawashima et al., 2007; Sakuno et al., 2011). To examine its dynamics in zygotic meiosis, we used heterothallic strains containing Ark1 tagged with GFP (Ark1-GFP) and tubulin tagged with mCherry. Ark1-GFP initially is visible during the transition from horse-tailing to metaphase I, with bright punctate foci which lasts for about 9 minutes (8.9’ ± 1.1’) localized at spindle poles (HT-MTI: -20 min) (**Fig. 7A, B, Fig. S8A)**. As cells move to metaphase I, there are discrete Ark1-GFP foci across the length of the spindle (HT-MTI: -10’ to 0’) (Kawashima et al., 2007) (**Fig. 7A, B)**. This scattered signal lasts for about 13 minutes (13.7’ ± 1.6’) (**Fig. S8A)**. At anaphase I Ark1-GFP signal re-localizes to the center of the extended spindles in the apparent midbody (**Fig. 7A-C, Fig. S8A)**.

This midzone Ark1 signal disappears after the completion of equational division after about 14 minutes (14.3' ± 2') (MTI-MI: 0 to 10 min) (**Fig. 7A, B, Fig. S8A)**. The signal intensity of Ark1-GFP increases to a maximum at anaphase1 **(Fig. S8B)**. Ark1 briefly disappears for about 13 minutes (13.4' ± 1.7') before showing similar dynamics in meiosis II: reappearance of foci during prophase II for 8 minutes (8.3' ± 1.3'), redistributions to the centromeres during metaphase II for 17 minutes (17.7'± 1.5') and back to midbody on the spindles during anaphase II for 9 minutes (8.9' ± 1.1') following the similar pattern as observed in meiosis I (MI-MII: 30 to 60 min) (**Fig. 7A, B, Fig. S8A)**. Ark1-GFP signal disappears after the completion of sister chromatid segregation (**Fig. 7A, B, Fig. S8B)**.

Bub1 is a centromere-associated conserved serine/threonine kinase, required for the protection of meiotic centromeric cohesion (Bernard et al., 2001; Marston and Wassmann, 2017). Bub1 regulates Sgo1's localization to the pericentromeric region (Kitajima et al., 2004). Previously, Bub1 dynamics were examined in *pat1* synchronized meiosis but how it behaves in an unperturbed heterothallic meiosis was not tested (Bernard et al., 2001; Miyazaki et al., 2017). Bub1-GFP initially appears as a single bright focus in the late horse-tailing stage (HT-MTI: -20') which likely localizes at the centromere. It remains visible for about 18 minutes (18.3' ± 2.3') in late horse-tailing, prior to metaphase I, and then the single focus converts in multiple foci distributed across the chromatin at metaphase I (**Fig. 7D, E, Fig. S8C)**. In metaphase I, Bub1-GFP signal intensity increases drastically and foci remain distributed across the spindle for about 11 minutes (11.4' ± 1.2') (HT-MTI: -10' to 0') (**Fig. 7D, E, Fig. S8C, D)**. As cells move to meiosis I, the signal diffuses from the chromatin to coalesce at a single focus on both daughter nuclei at spindle pole bodies representing the enrichment of Bub1 at the kinetochores (MTI-MI: 0 to 10 min) (**Fig. 7D, E)** (Miyazaki et al., 2017). This stage lasts for 10 minutes (10.3' ± 0.5') (**Fig. S8C)**. The signal disappears after the completion of anaphase I, reappearing after 20 minutes (20.9' ± 1.7') in late meiosis I/prophase II when again it appears in puncta (likely centromeres) for about 10 minutes (10.3' ± 0.6') (**Fig. 7D, E, Fig. S8C)**. As cells enter in metaphase II, the signal diffuses and distributes across the spindle in the same fashion as in metaphase I (MI-MII: 40 to 60 min) (**Fig. 7D-F)**. In this state, Bub1-GFP signals remain visible for 18 minutes (18.9' ± 1.4') before

disappearing during anaphase II (**Fig. S8C)**. We did not see any Bub1-GFP signal during the meiosis II.

Discussion

Typically, investigators describe the behavior of one or a few novel proteins during meiosis, but protocols vary from lab to lab. In many cases, investigators make use of the *pat1-114* temperature sensitive mutant (Beach et al., 1985; Iino and Yamamoto, 1985a; Iino and Yamamoto, 1985b; Nurse, 1985) which can induce a synchronous meiosis from haploid or diploid cells in response to temperature shift. However, *pat1* driven meiosis has notable differences from a normal zygotic meiosis, and these are are exacerbated in haploid meiosis compared to diploids (e.g., (Bähler et al., 1991; Pankratz and Forsburg, 2005; Yamamoto and Hiraoka, 2003). Additionally, many studies employ “snapshots” of different timepoints, rather than continuous observations with live cell imaging that reveal dynamic and brief events. We have established a standardized protocol for imaging meiosis over time in normal homothallic or heterothallic strains, which we employed previously (Escorcia et al., 2019). We chose representative proteins involved in different stages of meiosis, and compared their signal intensity, localization, and dynamics against a standard panel of meiotic nuclear events including karyogamy, horsetail formation, and MI and MII divisions. This allows direct comparison of localization and timing for representatives of different stages of meiosis.

Our observations of H3 histone (Hht1-mRFP/GFP) dynamics generally agree with those of other live-cell studies (Ding et al., 2006; Escorcia and Forsburg, 2017; Fennell et al., 2015; Klutstein et al., 2015; Tomita et al., 2013; Yamamoto et al., 2019; Yang et al., 2015). The timing from fusion to meiosis II takes approximately 4 ½ hours, which is in line with previous reports (Ding et al., 2006; Moiseeva et al., 2017; Tomita et al., 2013). Fission yeast spends a substantial amount of this time in prophase activities that take place during horse-tailing. The histone dynamics form a timer that we used to compare different strains.

We observed that predictable changes in nuclear mass correlate with changes that define functional shifts in different markers of meiotic progression. Importantly,

changes of Hht1 dynamics are an important monitor for perturbations, such as disruptions in DNA replication and repair (e.g., (Escorcia and Forsburg, 2017; Mastro and Forsburg, 2014; Mastro et al., 2020)).

We also see a correlation between signal intensity changes and changes in nuclear size. Spikes of fluorescence intensity are observed during fusion and in each of the two metaphase steps preceding the meiotic divisions. This link is consistent with reports showing elevated histone content during DNA synthesis and increased nuclear condensation in metaphase (Chikashige et al., 2004; Choe et al., 1985; Ding et al., 2004; Takayama and Takahashi, 2007; Yokobayashi et al., 2003).

Unexpectedly, our study suggests that S phase actually initiates prior to nuclear fusion in normal zygotes. This is likely coordinated by trans-acting transcription factors that form after cell fusion (e.g.,(Vještica et al., 2018)). Previously, in a *pat1*- induced meiosis, it was suggested that DNA replication occurs at the beginning of the horsetail stage (Chikashige et al., 2004). However, we observe that punctate, pan-nuclear EGFP-Pcn1- foci that are typical of S phase (e.g., (Meister et al., 2007)) appear at the stage we call pre-fusion (PF), prior to karyogamy. We find that EGFP-Pcn1 at this pre-fusion stage forms punctate pan-nuclear foci which we infer represents early S phase (Meister et al., 2007). At karyogamy, EGFP-Pcn1 signal intensity reaches a maximum, and is distributed in punctate foci across the nucleus including the nucleolar region, which we define as early to mid S-phase. Diffusion of EGFP signal and localization of large bright foci and then smaller and fewer foci at the edge of the nucleus during horsetail stages we propose represents late S phase. Our results agree with a recent study by (Ruan et al., 2015a) who observed a similar Pcn1 dynamics in *h90 (*homothallic*) S. pombe* cells.

We see consistent results with another S phase marker. Tos4-GFP is a transcription factor that accumulates in the nucleus during the early S phase of the mitotic cell cycle (Bastos de Oliveira FM et al., 2012; Kiang et al., 2009; Kim et al., 2020; Shen and Forsburg, 2019). We see Tos4-GFP appear in the nucleus prior to karyogamy; this is particularly striking because the strain we used is heterozygous for Tos4-GFP, so we can see it appear in just one of the two nuclei. Tos4-GFP is distributed across the nucleus following karyogamy, and disappears relatively early in

horse-tailing, somewhat before the loss of the last PCNA foci. We conclude that Tos4 nuclear localization is an early meiotic S phase marker with similar dynamics to its behavior during mitosis (Kim et al., 2020). Together, these data indicate that S phase initiates prior to nuclear fusion.

The meiotic cohesin (Rec8-GFP) is one of the most dynamic proteins in meiosis. Rec8 is initially detected in cells that have not yet undergone karyogamy. This is consistent with ongoing S phase and recruitment of cohesin to newly replicating sister chromatids (Doll et al., 2008; Watanabe and Nurse, 1999; Watanabe et al., 2001). After nuclear fusion, Rec8-GFP fluorescence intensifies and colocalizes with Hht1-mRFP throughout the nucleus. From the beginning of horse-tailing until the end of metaphase I, cohesin content, timing, and movement are closely linked to those of H3 histone. This signal pattern is consistent with the nuclear organization function of Rec8 during recombination and metaphase I condensation (Ding et al., 2004; Ding et al., 2006; Ding et al., 2016). Consistent with prior observations, the signal changes as cells enter meiosis I, forming distinct foci that are resolved just before sister chromatid segregation in meiosis II (Escorcia and Forsburg, 2017; Le et al., 2013; Mastro et al., 2020; Watanabe and Nurse, 1999). We have shown previously that disruption of DNA replication dynamics changes the timing of Rec8 in these events (Escorcia and Forsburg, 2017; Le et al., 2013; Mastro and Forsburg, 2014; Mastro et al., 2020).

Similar to our observation with Rec8-GFP, the linear element protein Rec27-GFP is first observed in pre-fusion nuclei. We see a bright pan-nuclear signal that continues into horse-tailing, eventually forming a few discrete foci. Given our data with Pcn1 and Tos4 that shows signal in pre-fusion nuclei, we infer that Rec27 protein accumulates in pre-meiotic S phase. This is consistent with expression data suggesting Rec27 is expressed before premeiotic S phase (Mata et al., 2002). Studies using nuclear spreads have shown that Rec27 eventually forms distinct structures associated with linear elements (Davis et al., 2008). We observe that Rec27 foci representing LinE elimination begin to disappear as cells transition into metaphase I. This observation reflects the end of Rec27 function in chromosome alignment and recombination (Bähler et al., 1993; Davis et al., 2008; Ellermeier and Smith, 2005; Phadnis et al., 2015; Sakuno and

Watanabe, 2015). Since disruption of Rec27 dynamics is associated with chromosome mis-segregation (Escorcia and Forsburg, 2017), the time window before nuclear condensation suggests a promising phase in which to study the end of cross-over processing and chiasma resolution (Ding et al., 2004; Sharif et al., 2002).

Consistent with its role as protector of centromeric Rec8 degradation prior to meiosis I (Ishiguro et al., 2010; Kitajima et al., 2004; Kitajima et al., 2006), Sgo1-GFP foci emerge approximately 1 hour before homologs segregate. Our data agree with other studies showing Rec8-GFP is removed from chromosome arms but not the centromere, where Sgo1 localization prevents cleavage (Ishiguro et al., 2010; Mastro et al., 2020).

Moa1 is reported to localize in the central core of the centromere, where it interacts with Rec8, ensuring that sister chromatids face the same orientation prior to homolog separation (Kim et al., 2015; Miyazaki et al., 2017; Yokobayashi and Watanabe, 2005). We observe Moa1-GFP foci emerging in the HT-MT1 transition and remaining until right before meiosis I. The role of Moa1 in mono-orientation is evident from the separation of foci clusters that occurs as cells approach metaphase I. Before the first nuclear division, six foci are seen arranged in clusters of three following a trajectory toward opposite cell poles. This signal pattern is similar to that of Sgo1-GFP, thereby lending additional support to their functional association (Kitajima et al., 2004; Kitajima et al., 2006).

Proteins involved in replication and repair span the timing from pre-fusion to the initiation of MI. As is expected for a protein associated with DNA replication and recombination, Rad11-CFP shows signal patterns from pre-fusion to metaphase I that resemble those of Rec8 and Rec27. The signal is pan-nuclear during the time window when markers associated with DNA synthesis like Tos4-GFP and Pcn1-GFP are active. As cells enter horse-tailing, Rad11-CFP fluorescence follows the outline and movement of the nuclear mass (Hht1-mRFP). During the HT-MTI transition, Rad11-CFP foci appear but dissipate as the nucleus begins to contract. These foci co-localize with Rad52-YFP signal, following meiosis I, diffused pan-nuclear signal is observed, but disappears completely prior to meiosis II.

Rad52 is a recombination mediator that either promotes Rad51 or antagonizes Dmc1 binding to RPA-coated presynaptic filaments during recombination (Murayama et al., 2013; Muris et al., 1997; Octobre et al., 2008). Which recombinase follows Rad52 association with RPA largely determines recombination dynamics in meiotic prophase (Murayama et al., 2013). Our observations show that Rad52-YFP signal is dim and diffused throughout horse-tailing. Foci emerge and increase in intensity during the HT-MTI transition, but disappear like those of Rad11-CFP and Rec27-GFP before metaphase I.

The final group of proteins we studied are involved in microtubule dynamics and the spindle checkpoint. In *S. pombe* meiosis, microtubules play crucial roles from early stages including fusion and horse tailing (Katsumata et al., 2016). Our data are consistent with previous work showing a bundle of microtubules mobilizing in pre-fusion and karyogamy, forming a X-shaped structure (Ding et al., 1998). In the horse-tail stage, DNA synthesis concludes, and homologous chromosome pairing, and recombination take place (Hiraoka and Dernburg, 2009) (Ruan et al., 2015b). We observed similar Atb2 dynamics of meiotic prophase as reported in (Fennell et al., 2015; Yamamoto et al., 1999). Our data are consistent with previous findings suggesting three distinct steps in spindle elongation (Nabeshima et al., 1998; Sakuno et al., 2011; Yamamoto et al., 2008). In step1, mainly dominated by prophase, microtubules elongate, and Atb2 signal intensity increases. Step 2 is characterized by constant spindle length with increase in signal intensity representing metaphase. Step 3 represents anaphase events when microtubule elongates further leading to the edge of the cell.

Unlike metazoans, *S. pombe* has only one Aurora B like kinase (*Sp*Ark1) which is an essential protein. A component of the chromosome passenger complex linked to kinetochore function, Ark1 plays a crucial role in proper spindle formation, chromosome condensation, establishment of bipolar attachment, activation of spindle assembly checkpoints and chromosome segregation (Hauf et al., 2007; Kawashima et al., 2007; Matsuhara and Yamamoto, 2016; Petersen et al., 2001; Sakuno et al., 2011) Previous studies show Ark1 dynamics in mitotic and early meiotic stages but dynamics and timing in an unperturbed zygotic meiosis has not been described previously (Petersen et al.,

2001; Sakuno et al., 2011) Our results show that Ark1-GFP initially forms a punctate focus during prophase, colocalizes with spindle pole body, in agreement with previous reports (Hauf et al., 2007; Petersen et al., 2001; Sakuno et al., 2011). Metaphase is mainly characterized by smaller foci scattered across spindles and colocalizing with the centromeres. Sgo1 shows similar dynamics during prometaphase and metaphase and Ark1 colocalizes with Sgo1 at centromeres and SPBs (Kawashima et al., 2007; Petersen et al., 2001). The localization of Aurora kinase on peri-centromeres during prometaphase has been confirmed using ChIP (Morishita et al., 2001). During anaphase Ark1-GFP leaves centromeres and relocates to the central part of elongated spindle, the mid-zone membrane domain (MDM) (Petersen et al., 2001; Sakuno et al., 2011; Salas-Pino and Daga, 2019). Our Ark1 dynamics of meiosis II aligned with meiosis I and mitotic cell cycles (Hauf et al., 2007; Petersen et al., 2001; Sakuno et al., 2011; Salas-Pino and Daga, 2019).

Bub1 kinase is an essential component of the spindle assembly checkpoint (SAC) and plays an important role in centromeric cohesion protection and proper Sgo1 localization to the pericentromeric regions (Bernard et al., 2001; Kawashima et al., 2010; Kitajima et al., 2004). Bub1 also plays a crucial role in Ark1 localization to the centromere regions (Hauf et al., 2007; Kawashima et al., 2007; Kitajima et al., 2004). We observed similar nuclear dynamics for Bub1 as for Ark1 early in meiosis. Bub1 dynamics differ from Ark1 during anaphase: when Ark1 leaves centromeres and localizes to the midzone of spindle, Bub1 remains attached to the centromeres. Our result also showed different Bub1 dynamics during meiosis I and II, as it remains attached to the centromere in meiosis I, but we could not see any signal during meiosis II. This supports previous findings of Bub1's role in monopolar attachment (Hauf et al., 2007; Miyazaki et al., 2017).

Concluding remarks

Fission yeast is an excellent model for meiotic progression. From nuclear fusion to genome reduction, we present fluorescent signposts that define dynamic behavior of proteins during meiotic DNA synthesis, genomic fusion, chromosome alignment, genetic recombination, metaphase, and meiosis, using a consistent protocol. This live-cell

microscopy approach provides information about the change of protein abundance and localization during meiotic differentiation and establishes a common template to facilitate comparisons of different proteins. This should prove particularly helpful in mutant backgrounds to define the extent of perturbations. By capturing the timing of different meiotic events in the context of nuclear change, we provide a general atlas of reliable markers that can be used to study dynamics and disruptions of meiotic processes in *S. pombe*.

Materials and Methods

Yeast strains, culture and cell growth

General fission yeast culture condition, media compositions and strain constructions are used as described in (Sabatinos and Forsburg, 2010). Different fluorescently tagged *S. pombe* strains used in this study are listed in the supplementary Table S1. For live cell imaging, heterothallic cells were initially grown in 5 ml YES media at 32ºC for 12-16 hours. 100- 250 µl starter culture transferred to 5 ml EMM media containing appropriate supplements and grown at 32ºC until the culture reached a late log stage (OD_{595} =~0.8). Late log phase cells harvested at 3,000 rpm for 5 minutes. To remove any remaining nutrient from the culture, pellets were washed twice with Malt Extract (ME) media. Finally, heterothallic pellets resuspended in 10 ml ME media and incubated at 25°C for 12 to 16 hours at 50-60 rpm. From this starved mating culture, 1 ml culture harvested in microfuge tubes and used for live cell microscopy.

Fluorescence live-cell microscopy

Live cell imaging of meiotic events was performed as described in (Escorcia and Forsburg, 2017; Escorcia et al., 2019). Briefly, 1 ml mating culture harvested at 5,000 rpm for 30 seconds. Pellets were resuspended in 250 µl ME media. 10 µl of cell suspension spread on top of 2% agarose pad made with liquid sporulation media and sealed with VaLaP (Vaseline/ Lanolin/ Paraffin in a ratio 1:1:1 by weight). Live cell imaging was performed at 25°C (pre-calibrated chamber) on a Delta Vision Microscope (Applied Precision, GE Healthcare, Issaquah, WA) equipped with Olympus 60x/1.40

Plan-Apo objective lens, solid-state illuminator, and 12-bit Photo metrics CoolSNAP_HQ2 Charged-coupled device (CCD) camera. Different filter sets and exposure timings were used to excite and detect fluorescent proteins (Table 2). 13 optical *z*-sections of 0.5 µm step size were acquired for each field at 10-minutes intervals over 8 hours. Images were acquired, deconvolved and all z-stacks projected into a single-plane as maximum intensity projection by SoftWoRx Version 5.5.1 (GE, Issaquah, WA) software. Finally, the projected fluorescence images were fused with transmitted light images. Downstream processing and image analysis were done using Fiji (ImageJ) an open source image analysis software (Schindelin et al., 2012). Detailed description of image analysis is described in (Escorcia and Forsburg, 2017; Escorcia et al., 2019).

Statistical Analysis

For different marker metrics across time and timing of individual events, the mean with 95% CI is presented. For comparisons among time points per marker, significance was evaluated using an ordinary One-Way ANOVA (for matched data) followed by Tukey's post hoc test. GraphPad Prism 8.4.2 was used for statistical analysis and graphical representations of the data.

Acknowledgements We thank Julie Cooper, Gerry Smith, and Yoshi Watanabe for sharing strains. The members of the lab for helpful comments. Marc Green and Tara Mastro for guidance and mentorship. Rosalind Elsie Franklin and Percy Lavon Julian for scientific inspiration. Funding from NIGMS R35 GM118109 (SLF) and T32AG052374 (WE).

Competing Interests: The authors declare that they have no competing interests.

Funding NIGMS R35 GM118109 (SLF) and T32AG052374 (WE).

References

Adachi, Y., Toda, T., Niwa, O. and Yanagida, M. (1986). Differential expressions of essential and nonessential alpha-tubulin genes in Schizosaccharomyces pombe. *Mol. Cell. Biol.* **6**, 2168–2178.

Arroyo, M. P., Downey, K. M., So, A. G. and Wangt, T. S. F. (1996). Schizosaccharomyces pombe proliferating cell nuclear antigen mutations affect DNA polymerase δ processivity. *J. Biol. Chem.* **271**, 15971–15980.

Bähler, J., Schuchert, P., Grimm, C. and Kohli, J. (1991). Synchronized meiosis and recombination in fission yeast: observations with pat1-114 diploid cells. *Curr. Genet.* **19**, 445–451.

Bähler, J., Wyler, T., Loidl, J. and Kohli, J. (1993). Unusual nuclear structures in meiotic prophase of fission yeast: a cytological analysis. *J. Cell Biol.* **121**, 241–256.

Bastos de Oliveira FM, MR, H., Brazauskas, P., Bruin RA, D. and MB, S. (2012). Linking DNA replication checkpoint to MBF cell-cycle transcription reveals a distinct class of G1/S genes. *EMBO J.* **31**, 1798–1810.

Beach, D., Rodgers, L. and Gould, J. (1985). ran1+ controls the transition from mitotic division to meiosis in fission yeast. *Curr. Genet.* **10**, 297–311.

Bernard, P., Maure, J. F. and Javerzat, J. P. (2001). Fission yeast Bub1 is essential in setting up the meiotic pattern of chromosome segregation. *Nat. Cell Biol.* **3**, 522–526.

Boehm, E. M., Gildenberg, M. S. and Washington, M. T. (2016). Chapter Seven - The Many Roles of PCNA in Eukaryotic DNA Replication. In *DNA Replication Across Taxa* (ed. Kaguni, L. S.) and Oliveira, M. T. B. T.-T. E.), pp. 231–254. Academic Press.

Carmena, M., Wheelock, M., Funabiki, H. and Earnshaw, W. C. (2012). The chromosomal passenger complex (CPC): From easy rider to the godfather of mitosis. *Nat. Rev. Mol. Cell Biol.* **13**, 789–803.

Cavalier-smith, T. (2002). Origins of the machinery of recombination and sex. *Heredity (Edinb).* **88**, 125–141.

Chikashige, Y., Kurokawa, R., Haraguchi, T. and Hiraoka, Y. (2004). Meiosis induced by inactivation of Pat1 kinase proceeds with aberrant nuclear positioning of centromeres in the fission yeast Schizosaccharomyces pombe. *Genes to Cells* **9**,

671–684.

Choe, K. N. and Moldovan, G.-L. (2017). Forging Ahead through Darkness: PCNA, Still the Principal Conductor at the Replication Fork. *Mol. Cell* **65**, 380–392.

Choe, J., Schuster, T. and Grunstein, M. (1985). Organization, primary structure, and evolution of histone H2A and H2B genes of the fission yeast Schizosaccharomyces pombe. *Mol. Cell. Biol.* **5**, 3261–3269.

Cooper, J. P., Watanabe, Y. and Nurse, P. (1998). Fission yeast Taz1 protein is required for meiotic telomere clustering and recombination. *Nature* **392**, 828–831.

Davis, L. and Smith, G. R. (2001). Meiotic recombination and chromosome segregation in Schizosaccharomyces pombe. *Proc. Natl. Acad. Sci. U. S. A.* **98**, 8395–8402.

Davis, L., Rozalén, A. E., Moreno, S., Smith, G. R. and Martín-Castellanos, C. (2008). Rec25 and Rec27, Novel Linear-Element Components, Link Cohesin to Meiotic DNA Breakage and Recombination. *Curr. Biol.* **18**, 849–854.

Ding, D. Q., Chikashige, Y., Haraguchi, T. and Hiraoka, Y. (1998). Oscillatory nuclear movement in fission yeast meiotic prophase is driven by astral microtubules, as revealed by continuous observation of chromosomes and microtubules in living cells. *J. Cell Sci.* **111**, 701–712.

Ding, D.-Q., Yamamoto, A., Haraguchi, T. and Hiraoka, Y. (2004). Dynamics of homologous chromosome pairing during meiotic prophase in fission yeast. *Dev. Cell* **6**, 329–341.

Ding, D.-Q., Sakurai, N., Katou, Y., Itoh, T., Shirahige, K., Haraguchi, T. and Hiraoka, Y. (2006). Meiotic cohesins modulate chromosome compaction during meiotic prophase in fission yeast. *J. Cell Biol.* **174**, 499–508.

Ding, D. Q., Haraguchi, T. and Hiraoka, Y. (2016). A cohesin-based structural platform supporting homologous chromosome pairing in meiosis. *Curr. Genet.* **62**, 499–502.

Doll, E., Molnar, M., Cuanoud, G., Octobre, G., Latypov, V., Ludin, K. and Kohli, J.

(2008). Cohesin and Recombination Proteins Influence the G 1 -to-S Transition in Azygotic Meiosis in Schizosaccharomyces pombe. *Genetics* **180**, 727–740.

Ellermeier, C. and Smith, G. R. (2005). Cohesins are required for meiotic DNA breakage and recombination in Schizosaccharomyces pombe. *Proc. Natl. Acad. Sci. U. S. A.* **102**, 10952–10957.

Escorcia, W. and Forsburg, S. L. (2017). Destabilization of the replication fork protection complex disrupts meiotic chromosome segregation. *Mol. Biol. Cell*.

Escorcia, W., Shen, K. F., Yuan, J. P. and Forsburg, S. L. (2019). Examination of mitotic and meiotic fission yeast nuclear dynamics by fluorescence live-cell microscopy. *J. Vis. Exp.*

Fennell, A., Fernández-álvarez, A., Tomita, K. and Cooper, J. P. (2015). Telomeres and centromeres have interchangeable roles in promoting meiotic spindle formation. *J. Cell Biol.* **208**, 415–428.

Galander, S., Barton, R. E., Borek, W. E., Spanos, C., Kelly, D. A., Robertson, D., Rappsilber, J. and Marston, A. L. (2019). Reductional Meiosis I Chromosome Segregation Is Established by Coordination of Key Meiotic Kinases. *Dev. Cell* **49**, 526-541.e5.

Gray, S. and Cohen, P. E. (2016). Control of Meiotic Crossovers: From Double-Strand Break Formation to Designation. *Annu. Rev. Genet.* **50**, 175–210.

Green, M. D., Sabatinos, S. A. and Forsburg, S. L. (2015). Microscopy Techniques to Examine DNA Replication in Fission Yeast. In *Methods in molecular biology (Clifton, N.J.)*, pp. 13–41. United States.

Hauf, S., Biswas, A., Langegger, M., Kawashima, S. A., Tsukahara, T. and Watanabe, Y. (2007). Aurora controls sister kinetochore mono-orientation and homolog bi-orientation in meiosis-I. *EMBO J.* **26**, 4475–4486.

Hiraoka, Y. and Dernburg, A. F. (2009). The SUN Rises on Meiotic Chromosome Dynamics. *Dev. Cell* **17**, 598–605.

Hiraoka, Y., Ding, D.-Q., Yamamoto, A., Tsutsumi, C. and Chikashige, Y. (2000). Characterization of fission yeast meiotic mutants based on live observation of meiotic prophase nuclear movement. *Chromosoma* **109**, 103–109.

Hirose, Y., Suzuki, R., Ohba, T., Hinohara, Y., Matsuhara, H., Yoshida, M., Itabashi, Y., Murakami, H. and Yamamoto, A. (2011). Chiasmata Promote Monopolar Attachment of Sister Chromatids and Their Co-Segregation toward the Proper Pole during Meiosis I. *PLoS Genet.* **7**, e1001329.

Hochwagen, A. (2008). Meiosis. *Curr. Biol.* **18**, R641–R645.

Horak, C. E., Luscombe, N. M., Qian, J., Bertone, P., Piccirrillo, S., Gerstein, M. and Snyder, M. (2002). Complex transcriptional circuitry at the G1/S transition in Saccharomyces cerevisiae. *Genes Dev.* **16**, 3017–3033.

Huang, M. and Elledge, S. J. (2000). The FHA domain, a phosphoamino acid binding domain involved in the DNA damage response pathway. *Cold Spring Harb. Symp. Quant. Biol.* **65**, 413–421.

Hunter, N. (2015). Meiotic Recombination: The Essence of Heredity. *Cold Spring Harb. Perspect. Biol.* **7**, a016618.

Iino, Y. and Yamamoto, M. (1985a). Mutants of Schizosaccharomyces pombe which sporulate in the haploid state. *Mol. Gen. Genet. MGG* **198**, 416–421.

Iino, Y. and Yamamoto, M. (1985b). Negative control for the initiation of meiosis in Schizosaccharomyces pombe *Proc. Natl. Acad. Sci.* **82**, 2447 LP – 2451.

Ishiguro, T., Tanaka, K., Sakuno, T. and Watanabe, Y. (2010). Shugoshin–PP2A counteracts casein-kinase-1-dependent cleavage of Rec8 by separase. *Nat. Cell Biol.* **12**, 500–506.

Katsumata, K., Hirayasu, A., Miyoshi, J., Nishi, E., Ichikawa, K., Tateho, K., Wakuda, A., Matsuhara, H. and Yamamoto, A. (2016). A Taz1- and Microtubule-Dependent Regulatory Relationship between Telomere and Centromere Positions in Bouquet Formation Secures Proper Meiotic Divisions. *PLoS Genet.* **12**, 1–30.

Kawashima, S. A., Tsukahara, T., Langegger, M., Hauf, S., Kitajima, T. S. and Watanabe, Y. (2007). Shugoshin enables tension-generating attachment of kinetochores by loading Aurora to centromeres. *Genes Dev.* **21**, 420–435.

Kawashima, S. A., Yamagishi, Y., Honda, T., Lshiguro, K. I. and Watanabe, Y. (2010). Phosphorylation of H2A by Bub1 prevents chromosomal instability through localizing shugoshin. *Science (80-.).* **327**, 172–177.

Kiang, L., Heichinger, C., Watt, S., Bähler, J. and Nurse, P. (2009). Cyclin-dependent kinase inhibits reinitiation of a normal S-phase program during G2 in fission yeast. *Mol. Cell. Biol.* **29**, 4025–32.

Kim, J., Ishiguro, K., Nambu, A., Akiyoshi, B., Yokobayashi, S., Kagami, A., Ishiguro, T., Pendas, A. M., Takeda, N., Sakakibara, Y., et al. (2015). Meikin is a conserved regulator of meiosis-I-specific kinetochore function. *Nature* **517**, 466–471.

Kim, S. M., Tripathi, V. P., Shen, K. F. and Forsburg, S. L. (2020). Checkpoint regulation of nuclear Tos4 defines s phase arrest in fission yeast. *G3 Genes, Genomes, Genet.* **10**, 255–266.

Kitajima, T. S., Kawashima, S. A. and Watanabe, Y. (2004). The conserved kinetochore protein shugoshin protects centromeric cohesion during meiosis. *Nature* **427**, 510–517.

Kitajima, T. S., Sakuno, T., Ishiguro, K. I., Iemura, S. I., Natsume, T., Kawashima, S. A. and Watanabe, Y. (2006). Shugoshin collaborates with protein phosphatase 2A to protect cohesin. *Nature* **441**, 46–52.

Klutstein, M., Fennell, A., Fernández-Álvarez, A. and Cooper, J. P. (2015). The telomere bouquet regulates meiotic centromere assembly. *Nat. Cell Biol.* **17**, 458–469.

Lam, I. and Keeney, S. (2015). Mechanism and Regulation of Meiotic Recombination Initiation. *Cold Spring Harb. Perspect. Biol.* **7**, a016634.

Le, A. H., Mastro, T. L. and Forsburg, S. L. (2013). The C-terminus of S. pombe DDK

subunit Dfp1 is required for meiosis-specific transcription and cohesin cleavage. *Biol. Open* **2**, 728–738.

Marston, A. L. and Wassmann, K. (2017). Multiple duties for spindle assembly checkpoint kinases in meiosis. *Front. Cell Dev. Biol.* **5**,.

Mastro, T. L. and Forsburg, S. L. (2014). Increased meiotic crossovers and reduced genome stability in absence of Schizosaccharomyces pombe Rad16 (XPF). *Genetics* **198**, 1457–1472.

Mastro, T. L., Tripathi, V. P. and Forsburg, S. L. (2020). Translesion synthesis polymerases contribute to meiotic chromosome segregation and cohesin dynamics in S chizosaccharomyces pombe. *J. Cell Sci.* **133**, jcs238709.

Mata, J., Lyne, R., Burns, G. and Bähler, J. (2002). The transcriptional program of meiosis and sporulation in fission yeast. *Nat. Genet.* **32**, 143–147.

Matsuhara, H. and Yamamoto, A. (2016). Autophagy is required for efficient meiosis progression and proper meiotic chromosome segregation in fission yeast. *Genes to Cells* **21**, 65–87.

Meister, P., Taddei, A., Ponti, A., Baldacci, G. and Gasser, S. M. (2007). Replication foci dynamics: Replication patterns are modulated by S-phase checkpoint kinases in fission yeast. *EMBO J.* **26**, 1315–1326.

Miyazaki, S., Kim, J., Yamagishi, Y., Ishiguro, T., Okada, Y., Tanno, Y., Sakuno, T. and Watanabe, Y. (2017). Meikin-associated polo-like kinase specifies Bub1 distribution in meiosis I. *Genes to Cells* **22**, 552–567.

Mizuguchi, T., Barrowman, J. and Grewal, S. I. S. (2015). Chromosome domain architecture and dynamic organization of the fission yeast genome. *FEBS Lett.* **589**, 2975–2986.

Moiseeva, V., Amelina, H., Collopy, L. C., Armstrong, C. A., Pearson, S. R. and Tomita, K. (2017). The telomere bouquet facilitates meiotic prophase progression and exit in fission yeast. *Cell Discov.* **3**, 17041.

Morishita, J., Matsusaka, T., Goshima, G., Nakamura, T., Tatebe, H. and Yanagida, M. (2001). Bir1/Cut17 moving from chromosome to spindle upon the loss of cohesion is required for condensation, spindle elongation and repair. *Genes to Cells* **6**, 743–763.

Murayama, Y., Kurokawa, Y., Tsutsui, Y. and Iwasaki, H. (2013). Dual regulation of Dmc1-driven DNA strand exchange by Swi5-Sfr1 activation and Rad22 inhibition. *Genes Dev.* **27**, 2299–2304.

Muris, D. F. R., Vreeken, K., Schmidt, H., Ostermann, K., Clever, B., Lohman, P. H. M. and Pastink, A. (1997). Homologous recombination in the fission yeast Schizosaccharomyces pombe: different requirements for the rhp51 + , rhp54 + and rad22 + genes. *Curr. Genet.* **31**, 248–254.

Nabeshima, K., Nakagawa, T., Straight, A. F., Murray, A., Chikashige, Y., Yamashita, Y. M., Hiraoka, Y. and Yanagida, M. (1998). Dynamics of centromeres during metaphase-anaphase transition in fission yeast: Dis1 is implicated in force balance in metaphase bipolar spindle. *Mol. Biol. Cell* **9**, 3211–3225.

Nurse, P. (1985). Mutants of the fission yeast Schizosaccharomyces pombe which alter the shift between cell proliferation and sporulation. *Mol. Gen. Genet. MGG* **198**, 497–502.

Octobre, G., Lorenz, A., Loidl, J. and Kohli, J. (2008). The Rad52 Homologs Rad22 and Rti1 of Schizosaccharomyces pombe Are Not Essential for Meiotic Interhomolog Recombination, but Are Required for Meiotic Intrachromosomal Recombination and Mating-Type-Related DNA Repair. *Genetics* **178**, 2399–2412.

Ohkura, H. (2015). Meiosis: An Overview of Key Differences from Mitosis. *Cold Spring Harb. Perspect. Biol.* **7**, a015859.

Okamoto, S. ya, Sato, M., Toda, T. and Yamamoto, M. (2012). SCF ensures meiotic chromosome segregation through a resolution of meiotic recombination intermediates. *PLoS One* **7**, 1–9.

Pankratz, D. G. and Forsburg, S. L. (2005). Meiotic S-Phase Damage Activates Recombination without Checkpoint Arrest. *Mol. Biol. Cell* **16**, 1651–1660.

Parker, A. E., Clyne, R. K., Carr, A. M. and Kelly, T. J. (1997). The Schizosaccharomyces pombe rad11+ gene encodes the large subunit of replication protein A. *Mol. Cell. Biol.* **17**, 2381–2390.

Petersen, J., Paris, J., Willer, M., Philippe, M. and Hagan, I. M. (2001). The S. pombe aurora-related kinase Ark1 associates with mitotic structures in a stage dependent manner and is required for chromosome segregation. *J. Cell Sci.* **114**, 4371 LP – 4384.

Phadnis, N., Cipak, L., Polakova, S., Hyppa, R. W., Cipakova, I., Anrather, D., Karvaiova, L., Mechtler, K., Smith, G. R. and Gregan, J. (2015). Casein Kinase 1 and Phosphorylation of Cohesin Subunit Rec11 (SA3) Promote Meiotic Recombination through Linear Element Formation. *PLOS Genet.* **11**, e1005225.

Radcliffe, P., Hirata, D., Childs, D., Vardy, L. and Toda, T. (1998). Identification of novel temperature-sensitive lethal alleles in essential β-tubulin and nonessential α2-tubulin genes as fission yeast polarity mutants. *Mol. Biol. Cell* **9**, 1757–1771.

Riedel, C. G., Katis, V. L., Katou, Y., Mori, S., Itoh, T., Helmhart, W., Gálová, M., Petronczki, M., Gregan, J., Cetin, B., et al. (2006). Protein phosphatase 2A protects centromeric sister chromatid cohesion during meiosis I. *Nature* **441**, 53–61.

Ruan, K., Yamamoto, T. G., Asakawa, H., Chikashige, Y., Masukata, H., Haraguchi, T. and Hiraoka, Y. (2015a). Meiotic nuclear movements in fission yeast are regulated by the transcription factor Mei4 downstream of a Cds1-dependent replication checkpoint pathway. *Genes to Cells* **20**, 160–172.

Ruan, K., Yamamoto, T. G., Asakawa, H., Chikashige, Y., Kimura, H., Masukata, H., Haraguchi, T. and Hiraoka, Y. (2015b). Histone H4 acetylation required for chromatin decompaction during DNA replication. *Sci. Rep.* **5**, 1–10.

Sabatinos, S. a and Forsburg, S. L. (2010). *Molecular genetics of*

Schizosaccharomyces pombe. 2nd ed. Elsevier Inc.

Sabatinos, S. a, Green, M. D. and Forsburg, S. L. (2012). Continued DNA synthesis in replication checkpoint mutants leads to fork collapse. *Mol. Cell. Biol.* **32**, 4986–97.

Sabatinos, S. A., Ranatunga, N. S., Yuan, J.-P., Green, M. D. and Forsburg, S. L. (2015). Replication stress in early S phase generates apparent micronuclei and chromosome rearrangement in fission yeast. *Mol. Biol. Cell* **26**, 3439–3450.

Sakuno, T. and Watanabe, Y. (2015). Phosphorylation of Cohesin Rec11/SA3 by Casein Kinase 1 Promotes Homologous Recombination by Assembling the Meiotic Chromosome Axis. *Dev. Cell* **32**, 220–230.

Sakuno, T., Tada, K. and Watanabe, Y. (2009). Kinetochore geometry defined by cohesion within the centromere. *Nature* **458**, 852–858.

Sakuno, T., Tanaka, K., Hauf, S. and Watanabe, Y. (2011). Repositioning of aurora b promoted by chiasmata ensures sister chromatid mono-orientation in meiosis i. *Dev. Cell* **21**, 534–545.

Salas-Pino, S. and Daga, R. R. (2019). Spatiotemporal control of spindle disassembly in fission yeast. *Cell. Mol. Life Sci.* **76**, 3543–3551.

Schindelin, J., Arganda-Carreras, I., Frise, E., Kaynig, V., Longair, M., Pietzsch, T., Preibisch, S., Rueden, C., Saalfeld, S., Schmid, B., et al. (2012). Fiji: an open-source platform for biological-image analysis. *Nat. Methods* **9**, 676–82.

Sharif, W. D., Glick, G. G., Davidson, M. K. and Wahls, W. P. (2002). Distinct functions of S. pombe Rec12 (Spo11) protein and Recl12-dependent crossover recombination (chiasmata) in meiosis I; and a requirement for Rec12 in meiosis II. *Cell Chromosom.* **1**, 1–14.

Shen, K.-F. and Forsburg, S. L. (2019). Overlapping Roles in Chromosome Segregation for Heterochromatin Protein 1 (Swi6) and DDK in Schizosaccharomyces pombe *Genetics* **212**, 417 LP – 430.

Takayama, Y. and Takahashi, K. (2007). Differential regulation of repeated histone genes during the fission yeast cell cycle. *Nucleic Acids Res.* **35**, 3223–3237.

Tomita, K., Bez, C., Fennell, A. and Cooper, J. P. (2013). A single internal telomere tract ensures meiotic spindle formation. *EMBO Rep.* **14**, 252–260.

van den Bosch, M., Vreeken, K., Zonneveld, J. B. ., Brandsma, J. A., Lombaerts, M., Murray, J. M., Lohman, P. H. . and Pastink, A. (2001). Characterization of RAD52 homologs in the fission yeast Schizosaccharomyces pombe. *Mutat. Res. Repair* **461**, 311–323.

Vještica, A., Merlini, L., Nkosi, P. J. and Martin, S. G. (2018). Gamete fusion triggers bipartite transcription factor assembly to block re-fertilization. *Nature* **560**, 397–400.

Watanabe, Y. and Nurse, P. (1999). Cohesin Rec8 is required for reductional chromosome segregation at meiosis. *Nature* **400**, 461–464.

Watanabe, Y., Yokobayashi, S., Yamamoto, M. and Nurse, P. (2001). Pre-meiotic S phase is linked to reductional chromosome segregation and recombination. *Nature* **409**, 359–363.

Yamagishi, Y., Sakuno, T., Shimura, M. and Watanabe, Y. (2008). Heterochromatin links to centromeric protection by recruiting shugoshin. *Nature* **455**, 251–255.

Yamamoto, A. and Hiraoka, Y. (2003). Monopolar spindle attachment of sister chromatids is ensured by two distinct mechanisms at the first meiotic division in fission yeast. *EMBO J.* **22**, 2284–2296.

Yamamoto, A., West, R. R., McIntosh, J. R. and Hiraoka, Y. (1999). A Cytoplasmic Dynein Heavy Chain Is Required for Oscillatory Nuclear Movement of Meiotic Prophase and Efficient Meiotic Recombination in Fission Yeast . *J. Cell Biol.* **145**, 1233–1250.

Yamamoto, A., Kitamura, K., Hihara, D., Hirose, Y., Katsuyama, S. and Hiraoka, Y. (2008). Spindle checkpoint activation at meiosis I advances anaphase II onset via meiosis-specific APC/C regulation. *J. Cell Biol.* **182**, 277–288.

Yamamoto, T. G., Ding, D. Q., Nagahama, Y., Chikashige, Y., Haraguchi, T. and Hiraoka, Y. (2019). Histone H2A insufficiency causes chromosomal segregation defects due to anaphase chromosome bridge formation at rDNA repeats in fission yeast. *Sci. Rep.* **9**, 1–13.

Yamashita, A., Sakuno, T., Watanabe, Y. and Yamamoto, M. (2017). Synchronous induction of meiosis in the fission yeast schizosaccharomyces pombe. *Cold Spring Harb. Protoc.* **2017**, 717–720.

Yang, H. J., Asakawa, H., Haraguchi, T. and Hiraoka, Y. (2015). Nup132 modulates meiotic spindle attachment in fission yeast by regulating kinetochore assembly. *J. Cell Biol.* **211**, 295–308.

Yokobayashi, S. and Watanabe, Y. (2005). The Kinetochore Protein Moa1 Enables Cohesion-Mediated Monopolar Attachment at Meiosis I. *Cell* **123**, 803–817.

Yokobayashi, S., Yamamoto, M. and Watanabe, Y. (2003). Cohesins Determine the Attachment Manner of Kinetochores to Spindle Microtubules at Meiosis I in Fission Yeast. *Mol. Cell. Biol.* **23**, 3965–3973.

Zickler, D. and Kleckner, N. (1999). Meiotic Chromosomes: Integrating Structure and Function. *Annu. Rev. Genet.* **33**, 603–754.

Zickler, D. and Kleckner, N. (2015). of Homologs during Meiosis. *Cold Spring Harb. Lab. Press* 1,2.

Figure 1. Nuclear dynamics of Hht1 defines signposts for meiotic events. (A) Live-cell image of a heterothallic unperturbed zygotic meiotic cell carrying fluorescently tagged histone 3 (Hht1-mRFP) (5608 x 5609). Time lapse images were captured every 10 minutes for 8 hours and selected frames are shown. Panel showing hht1-mRFP dynamics during meiotic cycle encompassing pre-fusion (Pre-FS), karyogamy to meiosis II (MII). Meiotic signposts are defined as FS-HT (premeiotic events; FS-HT: -10' (Pre-fusion); FS-HT: 0' (Karyogamy); FS-HT: 10' (beginning of nuclear oscillation)); HT-MTI (Horsetail to metaphase I transition (HT-MTI: -20' to -10')); MTI (metaphase I (HT-MTI: 0')); MTI-MI (metaphase I to anaphase I transition (MTI-MI: 10')); MI (meiosis I); MI-MTII (meiosis I to metaphase II (MI-MTII: 10' to 40')) and MTII-MII (metaphase II to meiosis II (MTII-MII: 50' to 60')). Numbers are representing timing in minutes and the scale bars are equal to 5 µm. (B) The durations of Hht1-mRFP dynamics in different meiotic event. (C) Quantitation of Hht1-mRFP fluorescence intensity. For (C) metaphase I is considered as a t0 minutes. Timing t (-60) to t (-20) are representing horsetail stage. t0 + 10 to t0 + 50 is meiosis I while t0 + 60 representing meiosis II. More than 35 cells were analyzed from at least two independent movies. Average (mean) values of timing and fluorescence intensities are presented in (B) and (C) respectively. Significance was evaluated using one-way ANOVA followed by Tukey's post hoc test. Error bars represent 95% class intervals.

Figure 2. Nuclear dynamics of Pcn1 and Tos4 during meiotic S phase. (A) Live-cell image of heterothallic zygotic meiotic cell carrying EGFP tagged PCNA (EGFP-Pcn1) and mRFP tagged Hht1 (3050 x 5615). Time lapse images were captured every 10 minutes for 8 hours and selected frames are shown. Panel showing dynamics of EGFP-Pcn1 (column 1) and EGFP-Pcn1, Hht1-mRFP merged (column 2) during early meiotic events encompassing Pre-fusion (Pre-FS), Karyogamy (FS) and early horse-tailing (HT) stage. Column 3 is showing closeups of selected time points from column 2. Numbers represent timing in minutes and scale bars equal 5 µm. (B) Durations of EGFP-Pcn1 foci signal disappearance. (C) Quantitation of EGFP-Pcn1 fluorescence intensity. (D) Time lapse images of a heterothallic zygotic meiotic cells carrying Tos4-GFP and Hht1-mRFP (8848 x 5615). Panel showing dynamics of Tos4-GFP (column 1), Tos4-GFP and hht1-mRFP merged (column 2) during early meiotic events encompassing Pre-fusion

(Pre-FS), Karyogamy (FS) and early horse-tailing (HT) stage. Column 3 is a closeups of selected time points from column 2. Numbers represent timing in minutes and scale bars equal to 5 µm. (E) Durations of Tos4-GFP signal disappearance. (F) Quantitation of Tos4-GFP fluorescence intensity. For (C) and (F) karyogamy (t 0'), Pre-FS (t -10'), and horsetail (t 10' onwards). For estimating timing and signal intensity, n=9 (PCNA) and n=15 (Tos4) cells from at least two independent movies were analyzed. Data in (B), (C), (E) and (F) are representing mean values. Significance was evaluated using one-way ANOVA followed by Tukey's post hoc test. Error bars represent 95% class intervals.

Figure 3. Rec8 cohesin dynamics. (A-C) Time-lapse images of meiotic cells carrying Rec8-GFP and Hht1-mRFP (7748 x 7840) were captured every 10 minutes for 8 hours and selected frames are shown. Panel (A) Rec8-GFP and (B) merged Rec8-GFP Hht1-mRFP show cohesin dynamics during different meiotic events covering late horsetail (HT), metaphase I (MTI), meiosis I (MI), metaphase II (MTII) and meiosis II (MII). (C) Closeup images of selected time frames from panel (B). Numbers represent timing in minutes and scale bars equal 5 µm. (D) Durations of Rec8-GFP signal during metaphase I and meiosis I. (C) Quantitation of Rec8-GFP fluorescence intensity. More than 35 cells from at least two independent movies were analyzed. Data in (D) and (E) represents mean timing and fluorescence intensities respectively. Significance was evaluated using one-way ANOVA followed by Tukey's post hoc test. Error bars represent 95% class intervals.

Figure 4. Nuclear dynamics of a kinetochore regulator Moa1. (A-C) Time-lapse images of meiotic cells carrying Moa1-GFP and Hht1-mRFP (8047 x 8048) were captured every 10 minutes for 8 hours and selected frames are shown. Panel (A) Moa1-GFP and (B) merged Moa1-GFP Hht1-mRFP show nuclear dynamics during different meiotic events covering late horsetail (HT) to meiosis II (MII). (C) Closeup images of selected time frames from panel (B). Numbers represent timing in minutes and scale bars equal 5 µm. (D) Durations of Moa1-GFP foci during horsetails and metaphase I. (E) Quantitation of Moa1-GFP fluorescence intensity. More than 35 cells from at least two independent movies were analyzed. Data in (D) and (E) represents mean timing

and fluorescence intensities respectively. Significance was evaluated using one-way ANOVA followed by Tukey's post hoc test. Error bars represent 95% class intervals.

Figure 5. Dynamics of Rad11 and Rad52 proteins. (A-C) Time-lapse images of meiotic cells carrying Hht1-mRFP, Rad11-CFP and Rad52-YFP (7327 x 7328) were captured every 10 minutes for 8 hours and selected frames are shown. Panels (A) Rad11-CFP, (B) Rad52-YFP and (C) merged image of Hht1-mRFP, Rad11-CFP and Rad52-YFP, are showing dynamics of repair foci during different meiotic events encompassing horsetail (HT) to meiosis II (MII). Due to the space limitation, bright field and Hht1-mRFP panels are omitted and closeup image of merged panel are presented in Supplementary Fig S6. Numbers represent timing in minutes and scale bars equal 5 µm. More than 35 cells from at least two independent movies were analyzed.

Figure 6. Meiotic spindle (Atb2-mCherry) dynamics. (A-C) Time-lapse images of heterothallic unperturbed zygotic meiotic cells carrying fluorescently tagged histone (Hht1-GFP) and tubulin (Atb2-mCherry) (8055 x 8203) were captured every 10 minutes for 8 hours and selected frames are shown. Panel (A) Atb2-mCherry and (B) merged image of Atb2-mCherry Hht1-mRFP show spindle dynamics during different meiotic events covering different meiotic events from horse-tailing (HT) to meiosis II (MII). (C) Closeup images of selected time frames from panel (B). Numbers represent timing in minutes and scale bars equal 5 µm. (D) Quantitation of the length of microtubule. More than 35 cells from at least two independent movies were analyzed. Data in (D) represents mean of the microtubule length. Significance was evaluated using one-way ANOVA followed by Tukey's post hoc test. Error bars represent 95% class intervals.

Figure 7. Nuclear dynamics of Aurora B (Ark1) and Bub1 kinase. (A-E) Live-cell images of heterothallic unperturbed zygotic meiotic cells carrying fluorescently tagged (A-C) Aurora B kinase (Ark1-GFP) & microtubule (Atb2-mCherry) (8053 x 8056) and (D-F) SAC Bub1 kinase (Bub1-GFP) & microtubule (Atb2-mCherry) (8055 x 8067). Time-lapse images were captured every 10 minutes for 8 hours and selected frames are shown. Panel (A) Ark1-GFP and (B) merged image of Ark1-GFP, Atb2-mCherry (D) Bub1-GFP and (E) merged image of Bub1-GFP, Atb2-mCherry nuclear dynamics during different meiotic events encompassing different meiotic events from horse-tailing (HT) to

meiosis II (MII). Panel (C) and (E) are closeup images of selected time frames from panel (B) and (D) respectively. Numbers represent timing in minutes and scale bars equal 5 µm. More than 35 cells from at least two independent movies were analyzed. Quantitative data presented in figure S8.

Figure 8. Meiotic signposts. Model presenting a visual atlas of reliable meiotic proteins that can be used to study the nuclear dynamics and disruptions of different meiotic processes in *S. pombe.* Meiotic signposts encompass events including pre-fusion (PF), Karyogamy (FS), horse-tailing (HT), metaphase I (MTI), meiosis I (MI), metaphase II (MTII) and meiosis II (MII). Presence of different meiotic proteins during different meiotic signpost are presented.

Supplementary Figures:

Figure S1. Nuclear dynamics of Hht1 during meiotic events. (A) Panel shows a false color image of Figure 1(A) generated by using Fiji's "thermal" LUT to show a heatmap of mRFP signal intensity for better understanding of nuclear dynamics. Selected time frames from Figure 1 (A) covering different meiotic signposts i.e. FS-HT, HT-MTI, MTI, MTI-MI MI and MI-MII are chosen for optimal representation. Red in the heatmap are representing high mRFP intensity and highly r4eswcompacted nucleus. (B) Closeup panels showing Pre-FS, MTI, MI and MII events. The scale bars in (A) and (B) equal 5 µm. (C) Quantitation of Hht1-mRFP signal area. (D) The graph showing quantitation of nuclear size by using Feret's diameter function of Fiji. For (C) and (D), metaphase I is considered as a t0 minutes. Timing t (-60) to t (-20) are representing horsetail stage. t0+10 to t0+50 is meiosis I while t0+60 representing meiosis II. More than 35 cells were analyzed from at least two independent movies. Values in the graphs represents mean and error bars represent 95% class intervals. Significance was evaluated using one-way ANOVA followed by Tukey's post hoc test.

Figure S2. Rec8 cohesin dynamics during early meiotic stages. (A-C) Time-lapse images of meiotic cells carrying Rec8-GFP and Hht1-mRFP (7748 x 7840) captured every 10 minutes for 8 hours and selected frames are shown. Panel (A) Rec8-GFP and (B) merged Rec8-GFP Hht1-mRFP show cohesin dynamics during early meiotic events covering Pre-fusion (Pre-FS), Karyogamy (FS) and early horse-tailing (HT) stage. (C)

Closeup images of selected time frames from panel (B). Numbers represent timing in minutes and scale bars equal 5 µm.

Figure S3. Linear element Rec27 foci elimination. (A-C) Time-lapse images of meiotic cells carrying Rec27-GFP and Hht1-mRFP (7777 x 7779) were captured every 10 minutes for 8 hours and selected frames are shown. Panel (A) Rec27-GFP and (B) merged Rec27-GFP Hht1-mRFP show linear element dynamics during different meiotic events covering late horsetail (HT), metaphase I (MTI), meiosis I (MI), metaphase II (MTII) and meiosis II (MII). (C) Closeup images of selected time frames from panel (B). Numbers represent timing in minutes and scale bars equal 5 µm. (D) Durations of Rec27 foci elimination before metaphase I. (E) Quantitation of Rec27-GFP fluorescence intensity. More than 35 cells from at least two independent movies were analyzed. Data in (D) and (E) represents mean timing and fluorescence intensities respectively. Significance was evaluated using one-way ANOVA followed by Tukey's post hoc test. Error bars represent 95% class intervals.

Figure S4. Rec27 dynamics during premeiotic and meiotic stage. (A-C) Time-lapse images of meiotic cells carrying Rec27-GFP and Hht1-mRFP (7777 x 7779) were captured every 10 minutes for 8 hours and selected frames are shown. Panel (A) Rec27-GFP and (B) merged Rec27-GFP Hht1-mRFP show linear element dynamics during different meiotic events covering pre-fusion (Pre-FS), Karyogamy (FS), horsetail (HT), metaphase I (MTI), meiosis I (MI), metaphase II (MTII) and meiosis II (MII). (C) Closeup images of selected time frames from panel (B). Numbers represent timing in minutes and scale bars equal 5 µm. More than 35 cells from at least two independent movies were analyzed.

Figure S5. Nuclear dynamics of Shugoshin Sgo1. (A-C) Time-lapse images of meiotic cells carrying Sgo1-GFP and Hht1-mRFP (7864 x 7865) were captured every 10 minutes for 8 hours and selected frames are shown. Panel (A) Sgo1-GFP and (B) merged Sgo1-GFP Hht1-mRFP show nuclear dynamics during different meiotic events covering late horsetail (HT) to meiosis II (MII). (C) Closeup images of selected time frames from panel (B). Numbers represent timing in minutes and scale bars equal 5 µm. (D) Durations of Sgo1-GFP foci disappearance during metaphase I. (E) Quantitation of

Rec27-GFP fluorescence intensity. More than 35 cells from at least two independent movies were analyzed. Data in (D) and (E) represents mean timing and fluorescence intensities respectively. Significance was evaluated using one-way ANOVA followed by Tukey's post hoc test. Error bars represent 95% class intervals.

Figure S6. Rad11 and Rad52 repair foci. (A) Panels showing time-lapse images of meiotic cells carrying fluorescently tagged histone (Hht1-mRFP), RPA (Rad11-CFP) and Rad52 (Rad52-YFP) (7327 x 7328). Column1 representing the dynamics of repair foci during different meiotic events encompassing horsetail (HT) to meiosis II (MII). Column 2 is a closeup image of selected time points. Numbers represent timing in minutes and scale bars equal 5 µm. (B-C) Durations of (B) Rad11 and (C) Rad52 repair foci appearance and loss during horsetail and metaphase I stage. (D- E) Quantitation of (D) Rad11-CFP and (E) Rad52-YFP fluorescence intensity. More than 35 cells from at least two independent movies were analyzed. Data in (B-C and D-E) represents mean values of timing and fluorescence intensities respectively. Significance was evaluated using one-way ANOVA followed by Tukey's post hoc test. Error bars represent 95% class intervals.

Figure S7. Microtubule dynamics. (A) Panels showing live-cell images of meiotic cells carrying fluorescently tagged histone (Hht1-GFP) and microtubule (Atb2-mCherry) (8055 x 8203). Time lapse images were captured every 10 minutes for 8 hours and selected frames are shown. Row 1 (Atb2-mCherry) and 2 (merged image of Atb2-mCherry Hht1-mRFP) show microtubule dynamics during different premeiotic and meiotic events covering pre-fusion to meiosis II (MII). Row 3 is showing the closeup images of selected time frames of row 2. Numbers represent timing in minutes and scale bars equal 5 µm. (B) Durations of microtubule depolymerization and elongation during different meiotic stages covering late horsetail (HT) to meiosis II (MII). More than 35 cells from at least two independent movies were analyzed. Data represents mean timing of the microtubule dynamics. Significance was evaluated using one-way ANOVA followed by Tukey's post hoc test. Error bars represent 95% class intervals.

Figure S8. Aurora-B and Bub1 kinase dynamics. Panel (A) Ark1-GFP (8053 x 8056) and (C) Bub1-GFP (8055 x 8067) showing the duration of fluorescent signal dynamics

during different meiotic events. Panel (B) Ark1-GFP and (D) Bub1-GFP showing the quantitation of fluorescent intensities. For both Ark1 and Bub1 dynamics, more than 35 cells of each from at least two independent movies were analyzed. Values presented in (A, C) and (B, D) are the means of timing and fluorescent intensities respectively. Significance was evaluated using one-way ANOVA followed by Tukey's post hoc test. Error bars represent 95% class intervals.

Figure S8. Quantitation graphs of all the proteins analyzed in this meiosis atlas.

Movie 1: Live cell imaging of meiotic cells carrying fluorescently tagged histone 3 (Hht1-mRFP). Representative time lapse imaging of zygotic meiotic cells carrying hht1-mRFP. Hht1-mRFP is represented by false color magenta.

Movie 2: Live cell imaging of meiotic cells carrying fluorescently tagged histone 3 (Hht1-mRFP) and PCNA (EGFP-Pcn1). Representative time lapse imaging of zygotic meiotic cells carrying hht1-mRFP. Hht1-mRFP is represented by false color magenta and EGFP-Pcn1 is green.

Movie 3: Live cell imaging of meiotic cells carrying fluorescently tagged histone 3 (Hht1-mRFP) and Tos4 (Tos4-GFP). Representative time lapse imaging of zygotic meiotic cells carrying hht1-mRFP. Hht1-mRFP is represented by false color magenta and Tos4-GFPn1 is green.

Movie 4: Live cell imaging of meiotic cells carrying fluorescently tagged histone 3 (Hht1-mRFP) and Rec8 (Rec8-GFP). Representative time lapse imaging of zygotic meiotic cells carrying hht1-mRFP. Hht1-mRFP is represented by false color magenta and Rec8-GFP is green.

Movie 5: Live cell imaging of meiotic cells carrying fluorescently tagged histone 3 (Hht1-mRFP) and Rec27 (Rec27-GFP). Representative time lapse imaging of zygotic meiotic cells carrying hht1-mRFP. Hht1-mRFP is represented by false color magenta and Rec27-GFP is green.

Movie 6: Live cell imaging of meiotic cells carrying fluorescently tagged histone 3 (Hht1-mRFP) and Sgo1 (Sgo1-GFP). Representative time lapse imaging of zygotic meiotic cells carrying hht1-mRFP. Hht1-mRFP is represented by false color magenta and Sgo1-GFP is green.

Movie 7: Live cell imaging of meiotic cells carrying fluorescently tagged histone 3 (Hht1-mRFP) and Moa1 (Moa1-GFP). Representative time lapse imaging of zygotic meiotic cells carrying hht1-mRFP. Hht1-mRFP is represented by false color magenta and Moa1-GFP is green.

Movie 8: Live cell imaging of meiotic cells carrying fluorescently tagged histone 3 (Hht1-mRFP) RPA (Rad11-CFP) and Rad52 (Rad52-YFP). Representative time lapse imaging of zygotic meiotic cells carrying hht1-mRFP. Hht1-mRFP is represented by false color magenta, Rad11 is cyan and Rad52 is yellow.

Movie 9: Live cell imaging of meiotic cells carrying fluorescently tagged histone 3 (Hht1-GFP) and tubulin (Atb2-mCherry). Representative time lapse imaging of zygotic meiotic cells carrying Hht1-GFP. Hht1-GFP is represented by false color green and Atb2-mCherry is magenta.

Movie 10: Live cell imaging of meiotic cells carrying fluorescently tagged Aroura B (Ark1-GFP) and tubulin (Atb2-mCherry). Representative time lapse imaging of zygotic meiotic cells carrying Ark1-GFP. Ark1-GFP is represented by false color green and Atb2-mCherry is magenta.

Movie 11: Live cell imaging of meiotic cells carrying fluorescently tagged Bub1 (Bub1-GFP) and tubulin (Atb2-mCherry). Representative time lapse imaging of zygotic meiotic cells carrying Bub1-GFP. Bub1-GFP is represented by false color green and Atb2-mCherry is magenta.

Table S1. List of strains used in this study.

Strain	Genotype	Reference
3050	h+ leu1-32 ura4:: EGFP-pcn1+	Meister et al 2003
5608	h- hht1-mRFP: KanMX6 leu1-32 ura4-D18	Lab stock
5609	h+ hht1-mRFP:KanMX6 leu1-32 ura4-D18	Lab Stock
5615	h- hht1-mRFP: hphMX6 leu1-32 ura4-D18 his3-D1	Lab Stock
7327	h+ hht1-mRFP:KanMX6 rad11-Cerulean::hphMX rad22-YFP-natMX leu1-32 ade6-M210 ? ura4-D18	Lab Stock
7328	h- hht1-mRFP:KanMX6 rad11-Cerulean::hphMX rad22-YFP-natMX leu1-32 ade6-M210 ? ura4-D18	Lab Stock
7748	h- rec8-GFP:KanMX6 hht1-mRFP:KanMX6 pat1-114 ura4-D18 ade6-m216	Escorcia 2017
7840	h+ rec8-GFP:KanMX6 hht1-mRFP:KanMX6 pat1-114 ura4-D18 ade6-m216	Escorcia 2017
7777	h+ rec27-205-GFP-KanMX hht1-mRFP:KanMX6 pat1-114 ura4-D18 ade6-3049 lys4-95	Escorcia 2017
7779	h- rec27-205-GFP-KanMX hht1-mRFP:KanMX6 pat1-114 ura4-D18 ade6-3049 lys4-95	Escorcia 2017
7864	h- sgo1-FLAG:GFP hht1-mRFP:KanMX6 ura4-D18 leu? ade6-M210	Escorcia 2017
7865	h+ sgo1-FLAG:GFP hht1-mRFP:KanMX6 ura4-D18 leu? ade6-M210	Escorcia 2017
8047	h+ KanMX6-moa1-5'-GFP-3pk-moa1 hht1-mRFP:KanMX6 ura4-D18 leu1-32	Lab Stock
8048	h- KanMX6-moa1-5'-GFP-3pk-moa1 hht1-mRFP:KanMX6 ura4-D18 leu1-32	Lab Stock
8053	h+ ark1-GFP:KanR Z::Padh-mCherry-atb2:natR ade6-M210	Lab Stock
8055	h+ Z::Padh-mCherry-atb2:NatR ura4-D18 leu1-32	Lab Stock
8056	h- Z::Padh-mCherry-atb2:NatR ura4-D18	Lab Stock
8067	h- bub1-GFP::his3+ leu1-32 ade6-M210	Lab Stock
8203	h- hht1-GFP-ura4+ ura4-D18 leu1-32 ade6-M210	Lab Stock
8848	h+ Tos4-GFP::KanMX6 leu1-32 ura4-D18 ade6-M210 can1-1? his3-	Lab Stock

	D1D1	

Table S2. Timing of meiotic markers and descriptive statistics.

Table S3. Descriptive and comparative statistics of meiotic markers.

A

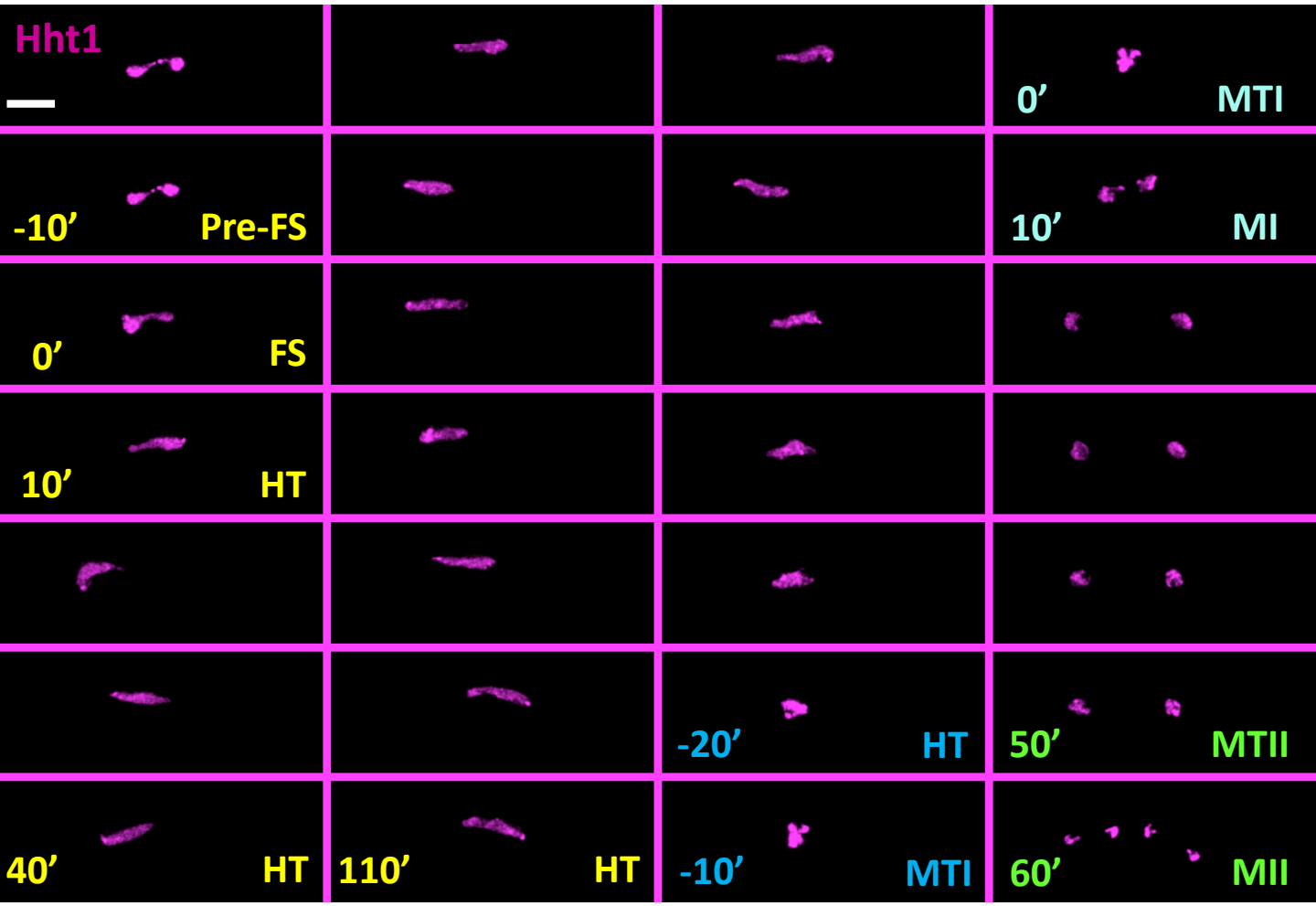
Hht1
0’
MTI
-10’
Pre-FS
10’
MI
0’
FS
10’
HT
-20’
HT
50’
MTII
40’
HT
110’
HT
-10’
MTI
60’
MII

B

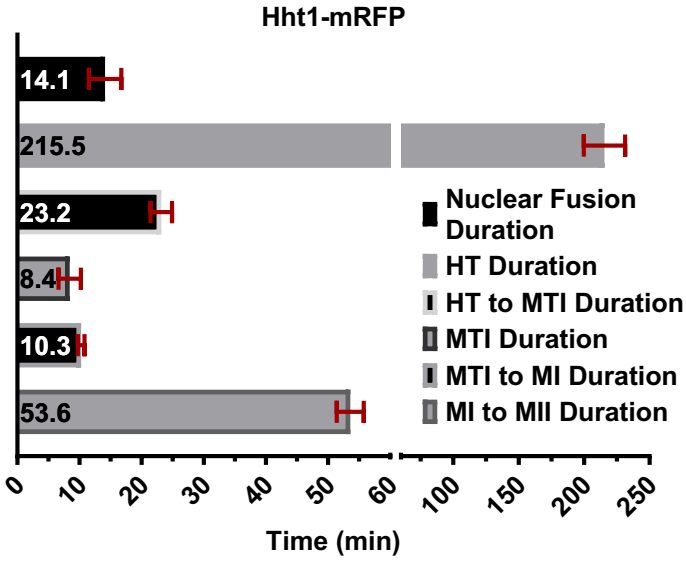
Hht1-mRFP
14.1
215.5
23.2
8.4
10.3
53.6
Nuclear Fusion Duration
HT Duration
HT to MTI Duration
MTI Duration
MTI to MI Duration
MI to MII Duration
0
10
20
30
40
50
60
100
150
200
250
Time (min)

C

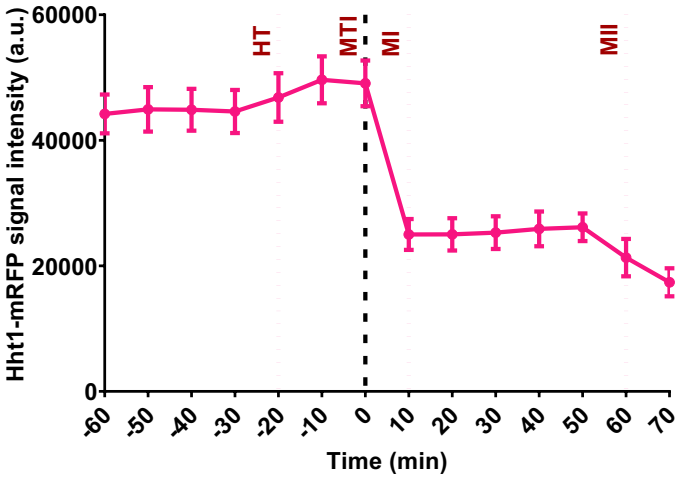
Hht1-mRFP signal intensity (a.u.)
60000
40000
20000
0
HT
MTI
MI
MII
-60
-50
-40
-30
-20
-10
0
10
20
30
40
50
60
70
Time (min)

Fig. 1

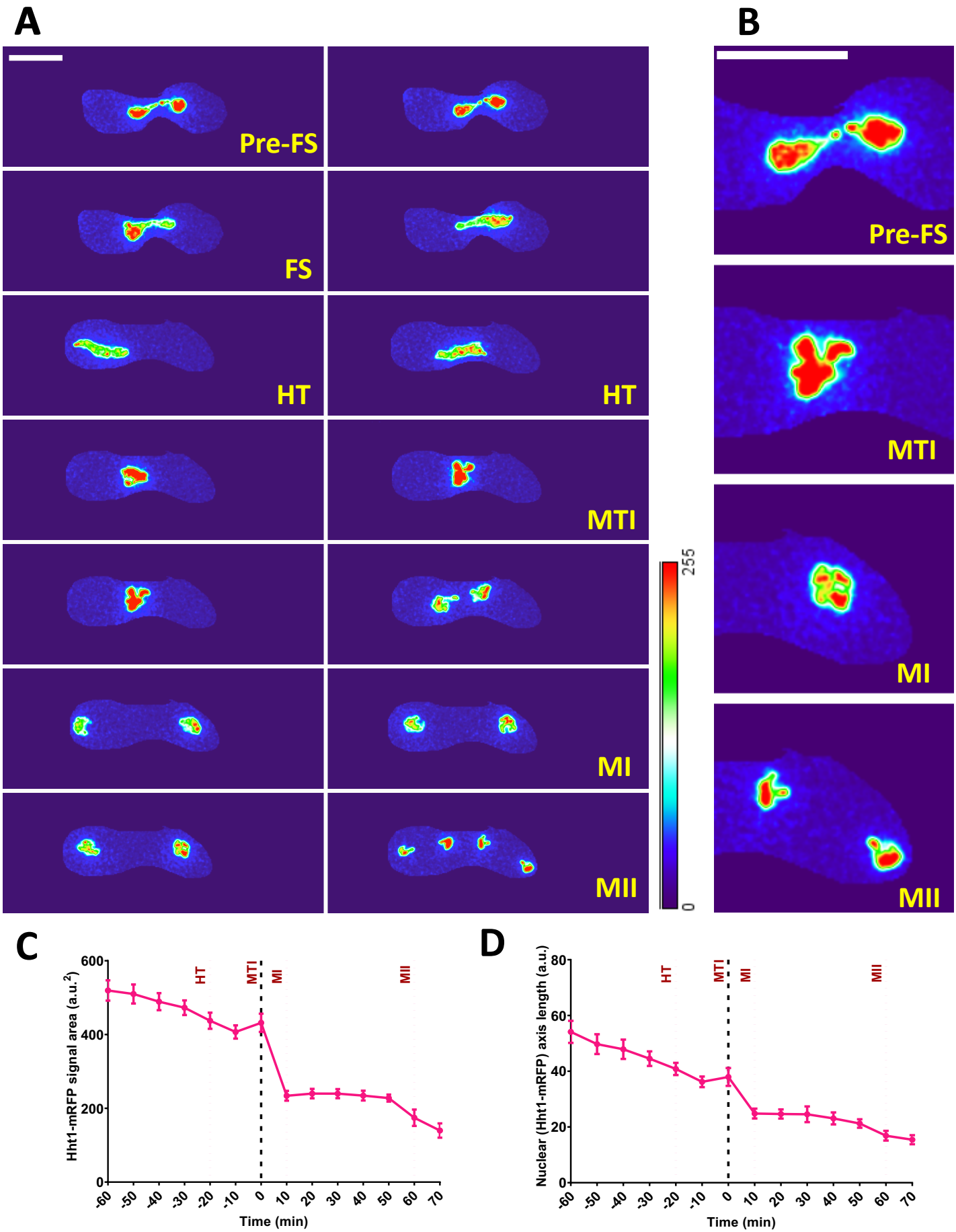
A
B
Pre-FS
FS
HT
HT
MTI
MI
MII
255
0
Pre-FS
MTI
MI
MII
C
Hht1-mRFP signal area (a.u.^{2})
600
400
200
0
HT
MTI
MI
MII
-60
-50
-40
-30
-20
-10
0
10
20
30
40
50
60
70
Time (min)
D
Nuclear (Hht1-mRFP) axis length (a.u.)
80
60
40
20
0
HT
MTI
MI
MII
-60
-50
-40
-30
-20
-10
0
10
20
30
40
50
60
70
Time (min)

Fig S1.

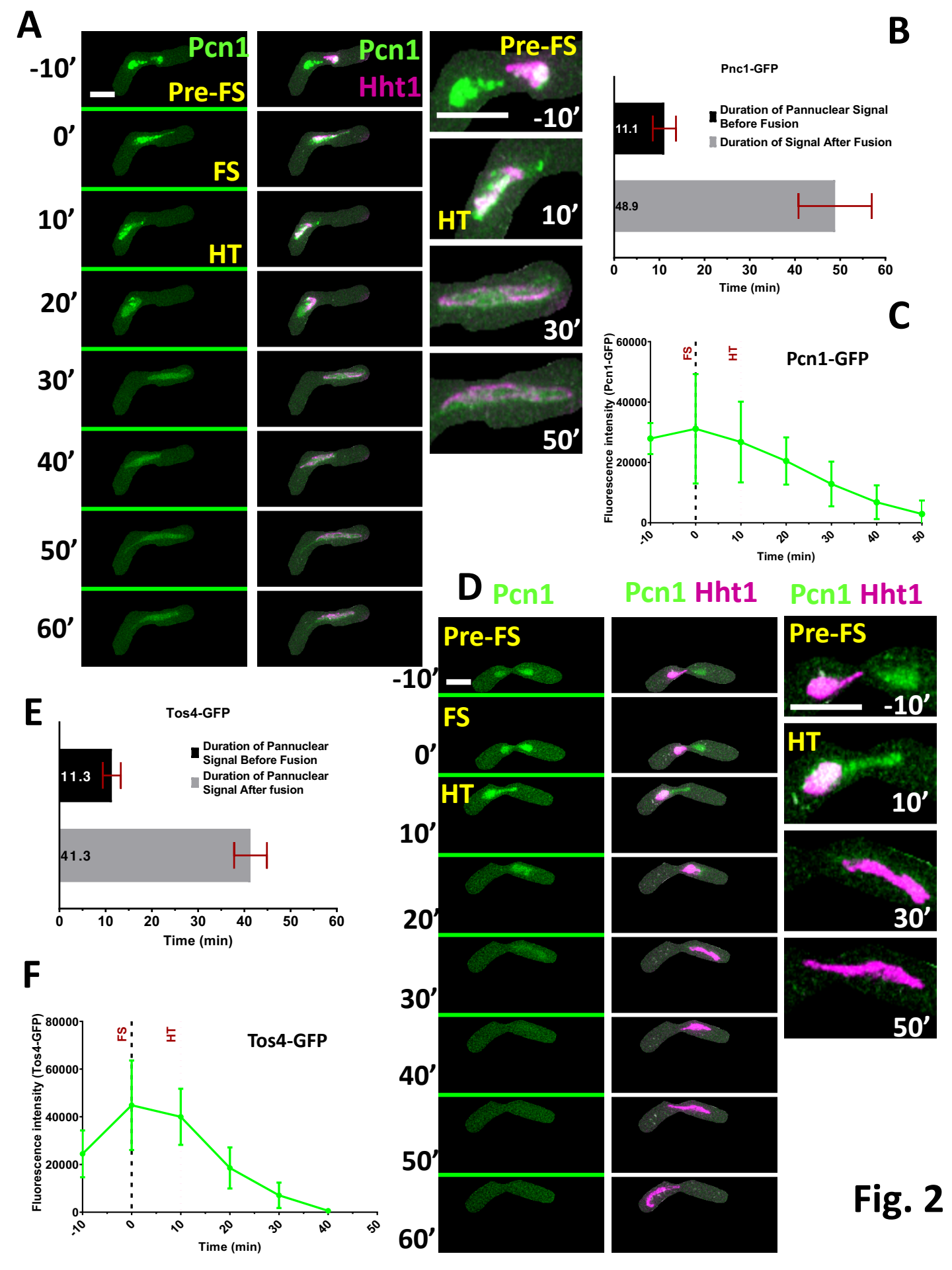
A
Pcn1
Pre-FS
Pcn1
Hht1
Pre-FS
-10'
0'
FS
10'
HT
20'
30'
40'
50'
60'
-10'
HT
10'
30'
50'
B
Pnc1-GFP
Duration of Pannuclear Signal Before Fusion
Duration of Signal After Fusion
11.1
48.9
0
10
20
30
40
50
60
Time (min)
C
Pcn1-GFP
FS
HT
Fluorescence intensity (Pcn1-GFP)
60000
40000
20000
0
-10
0
10
20
30
40
50
Time (min)
D
Pcn1
Pcn1 Hht1
Pcn1 Hht1
Pre-FS
FS
HT
-10'
0'
10'
20'
30'
40'
50'
60'
Pre-FS
HT
-10'
10'
30'
50'
E
Tos4-GFP
Duration of Pannuclear Signal Before Fusion
Duration of Pannuclear Signal After fusion
11.3
41.3
0
10
20
30
40
50
60
Time (min)
F
Tos4-GFP
FS
HT
Fluorescence intensity (Tos4-GFP)
80000
60000
40000
20000
0
-10
0
10
20
30
40
50
Time (min)

Fig. 2

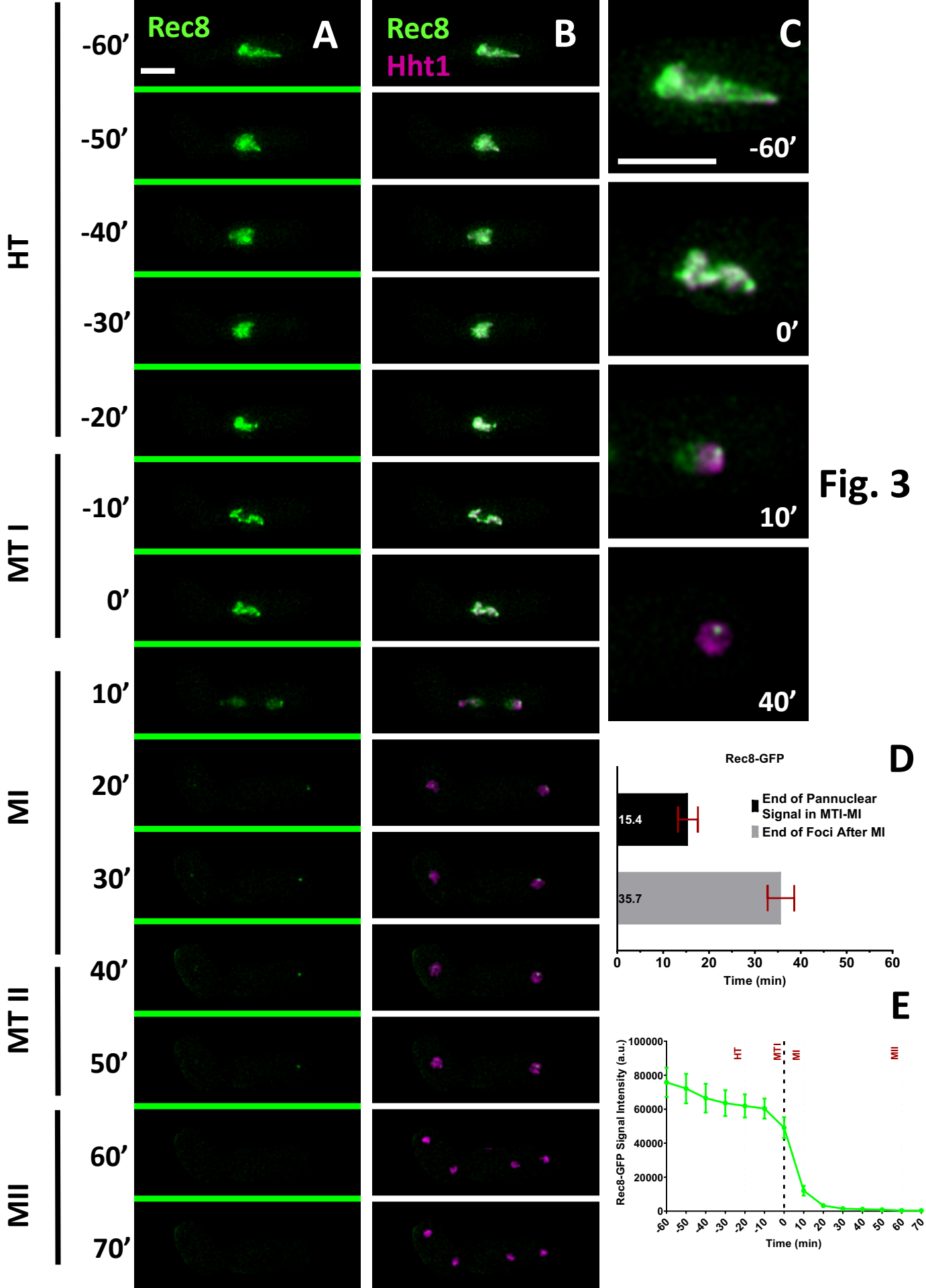
Rec8
A
Rec8
Hht1
B
C
-60'
-50'
-40'
-30'
-20'
-10'
0'
10'
20'
30'
40'
50'
60'
70'
HT
MT I
MI
MT II
MII
0'
10'
40'
Fig. 3
D
Rec8-GFP
End of Pannuclear Signal in MTI-MI
End of Foci After MI
15.4
35.7
0
10
20
30
40
50
60
Time (min)
E
Rec8-GFP Signal Intensity (a.u.)
100000
80000
60000
40000
20000
0
HT
MTI
MI
MII
-60
-50
-40
-30
-20
-10
0
10
20
30
40
50
60
70
Time (min)

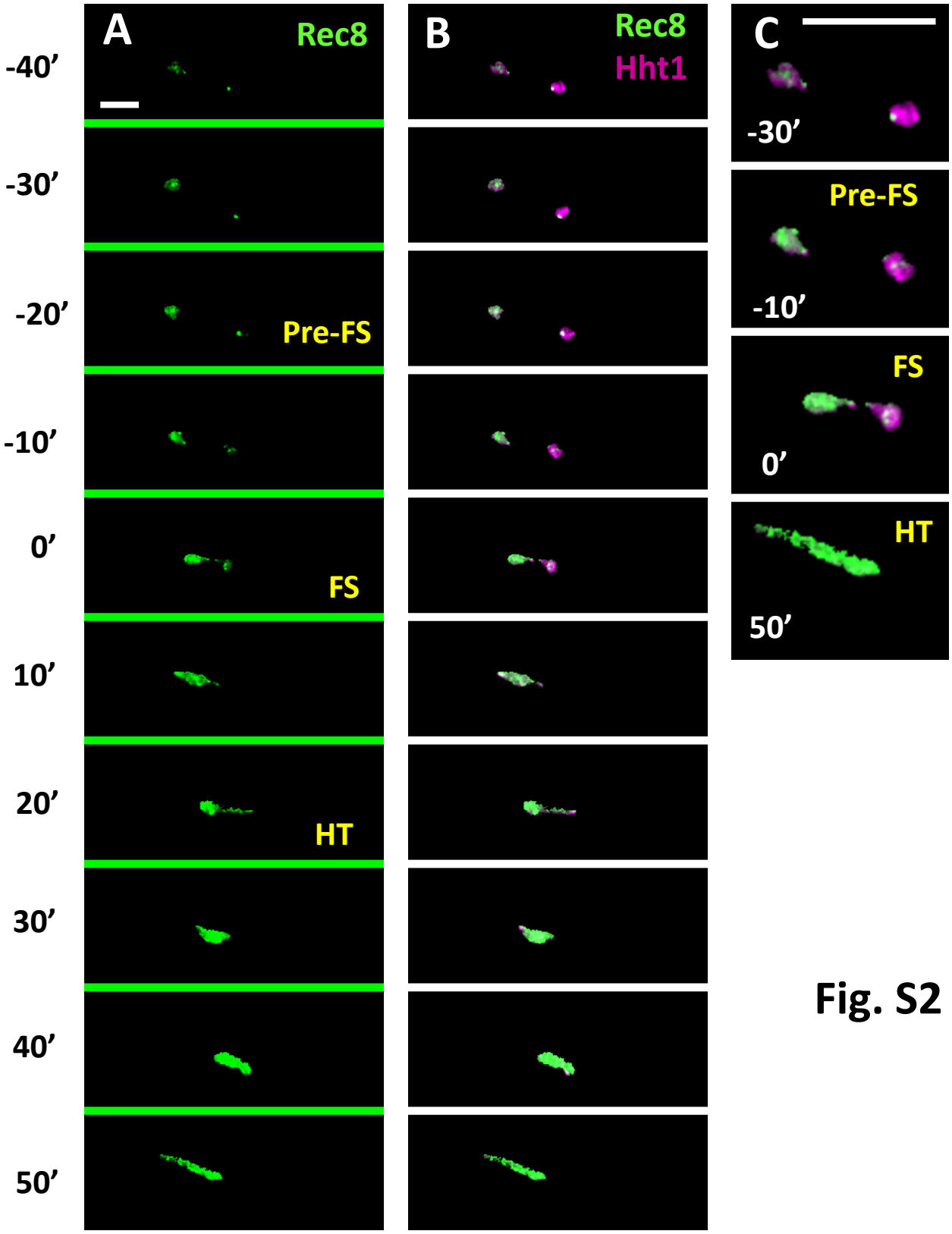
A
Rec8
B
Rec8
Hht1
C
-40'
-30'
-20'
-10'
0'
10'
20'
30'
40'
50'
Pre-FS
FS
HT
-30'
Pre-FS
-10'
FS
0'
HT
50'

Fig. S2

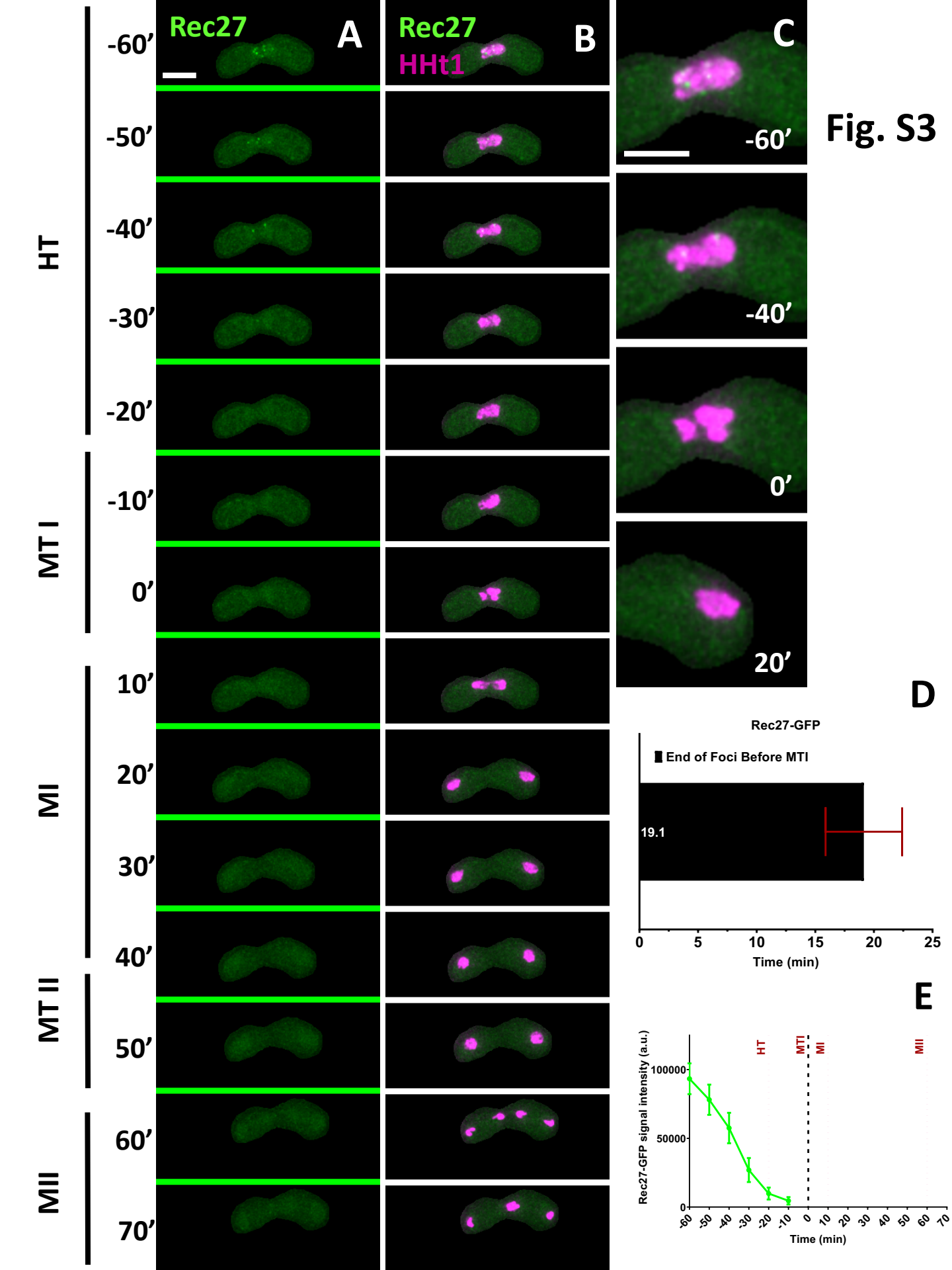
Fig. S3
A
Rec27
B
Rec27
HHt1
C
-60'
-40'
0'
20'
HT
MT I
MI
MT II
MII
-60'
-50'
-40'
-30'
-20'
-10'
0'
10'
20'
30'
40'
50'
60'
70'
D
Rec27-GFP
End of Foci Before MTI
19.1
0
5
10
15
20
25
Time (min)
E
Rec27-GFP signal intensity (a.u.)
100000
50000
0
HT
MTI
MI
MII
-60
-50
-40
-30
-20
-10
0
10
20
30
40
50
60
70
Time (min)

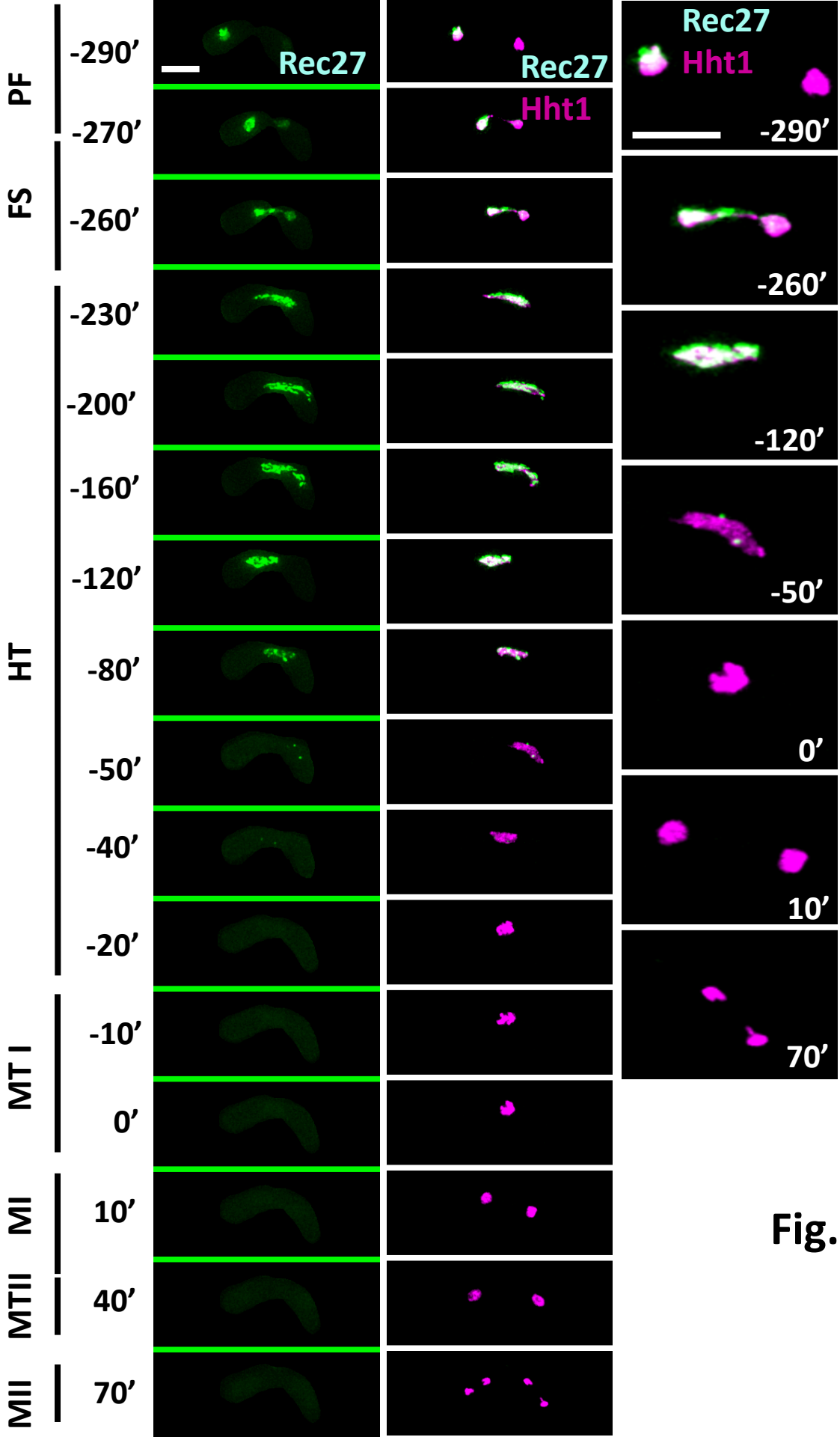
PF
FS
HT
MT I
MI
MTII
MII
-290'
-270'
-260'
-230'
-200'
-160'
-120'
-80'
-50'
-40'
-20'
-10'
0'
10'
40'
70'
Rec27
Rec27
Hht1
Rec27
Hht1
-290'
-260'
-120'
-50'
0'
10'
70'

Fig. S4

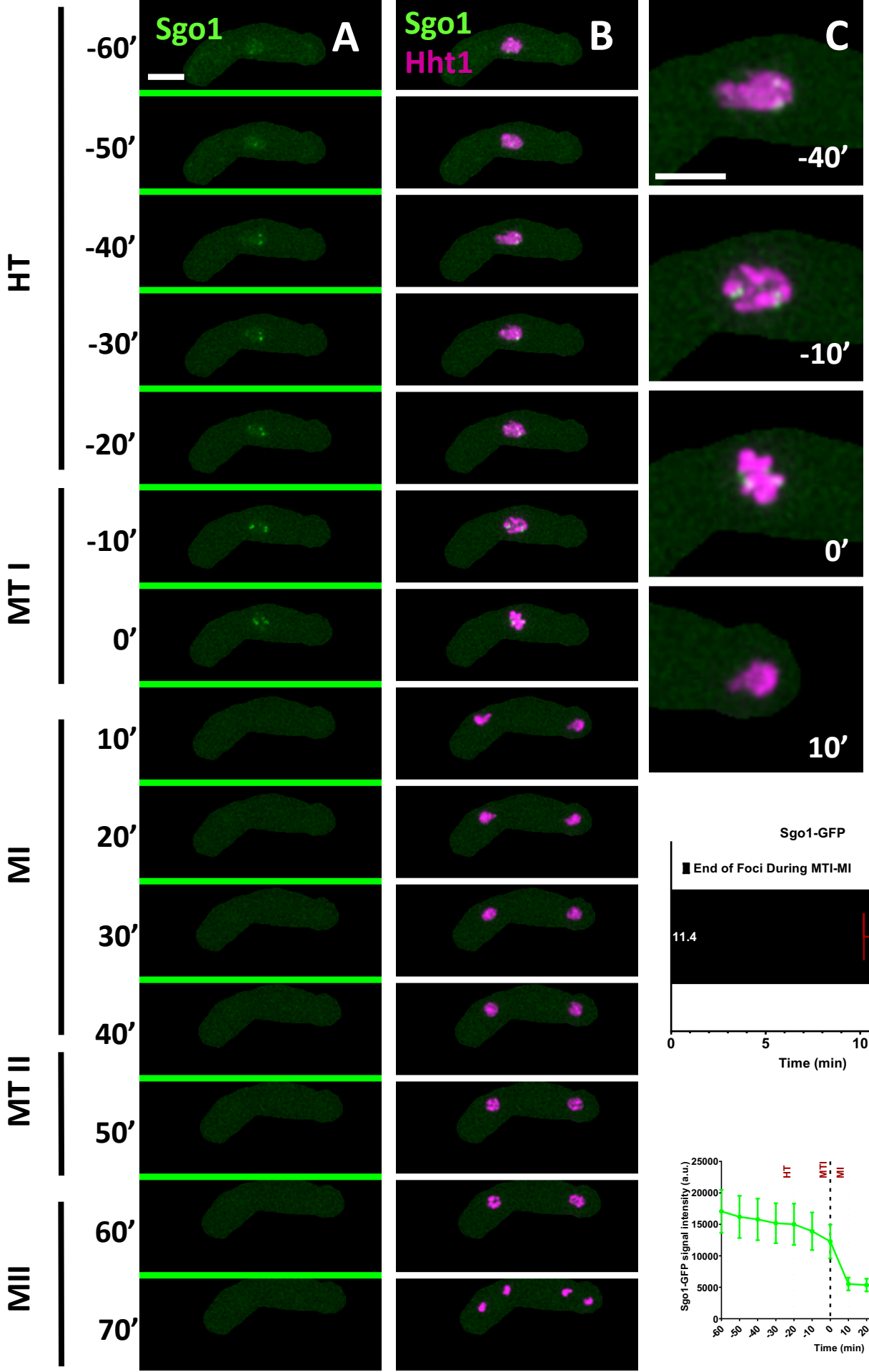
Sgo1
A
Sgo1
Hht1
B
C
-60'
-50'
-40'
-30'
-20'
-10'
0'
10'
20'
30'
40'
50'
60'
70'
HT
MT I
MI
MT II
MII
-40'
-10'
0'
10'
D
Sgo1-GFP
End of Foci During MTI-MI
11.4
0
5
10
15
Time (min)
E
Sgo1-GFP signal intensity (a.u.)
25000
20000
15000
10000
5000
0
HT
MTI
MI
MII
-60
-50
-40
-30
-20
-10
0
10
20
30
40
50
60
70
Time (min)

Fig. S5

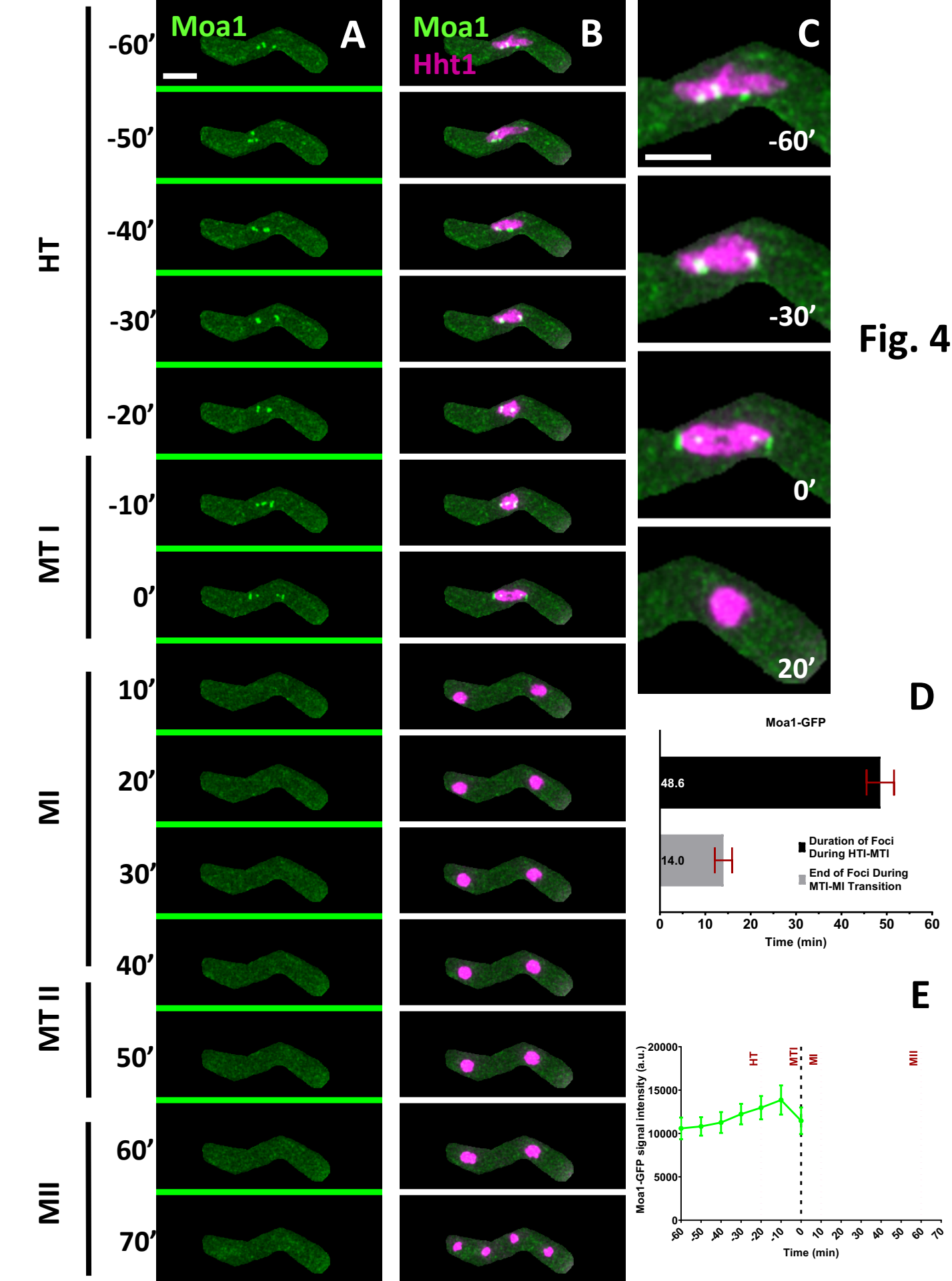
Moa1
A
Moa1
Hht1
B
C
-60'
-50'
-40'
-30'
-20'
-10'
0'
10'
20'
30'
40'
50'
60'
70'
HT
MT I
MI
MT II
MII
-60'
-30'
0'
20'
D
Moa1-GFP
48.6
14.0
Duration of Foci During HTI-MTI
End of Foci During MTI-MI Transition
0
10
20
30
40
50
60
Time (min)
E
Moa1-GFP signal intensity (a.u.)
20000
15000
10000
5000
0
HT
MTI
MI
MII
-60
-50
-40
-30
-20
-10
0
10
20
30
40
50
60
70
Time (min)

Fig. 4

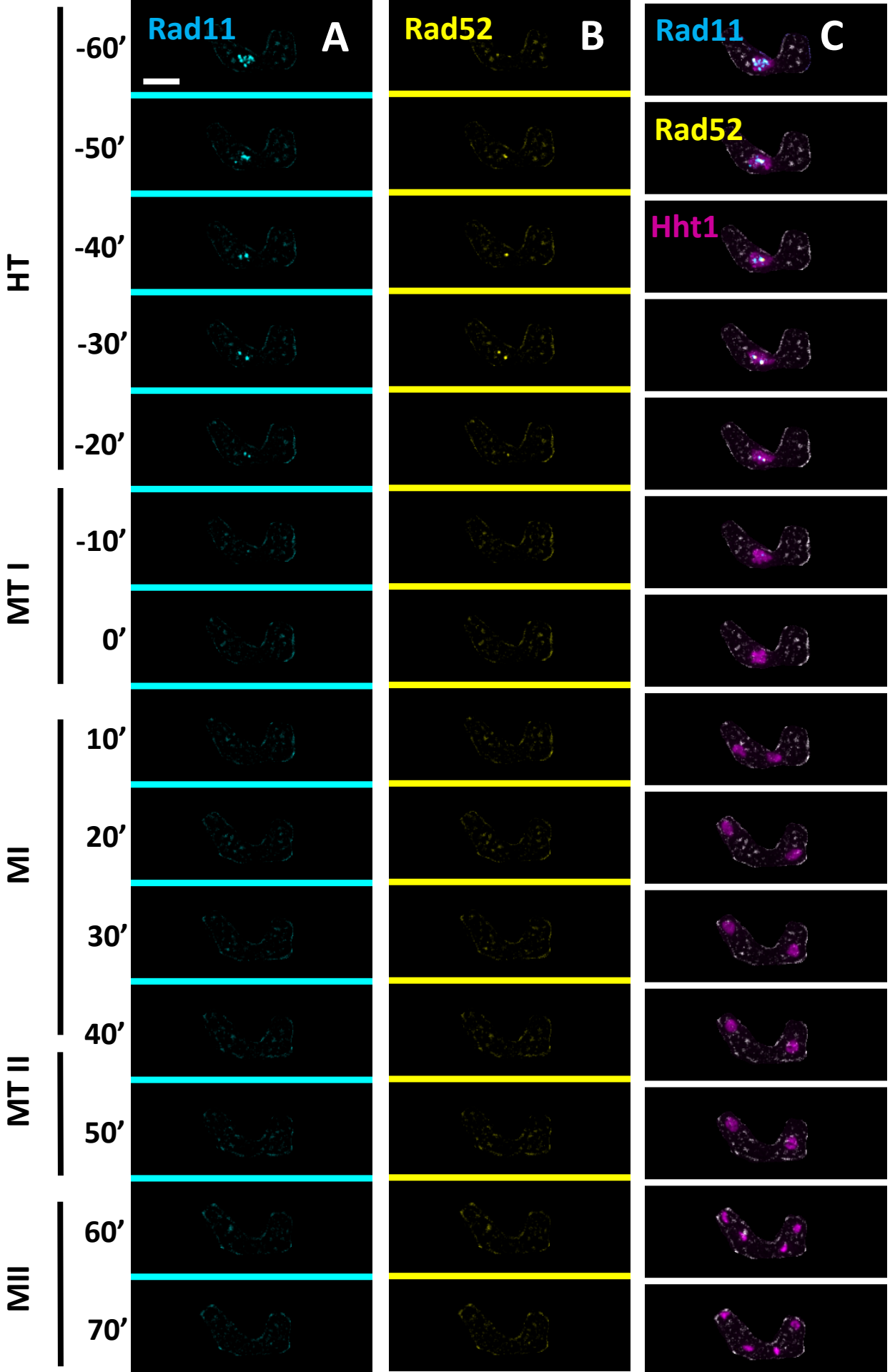
Rad11
A
Rad52
B
Rad11
C
Rad52
Hht1
HT
MT I
MI
MT II
MII
-60'
-50'
-40'
-30'
-20'
-10'
0'
10'
20'
30'
40'
50'
60'
70'

Fig. 5

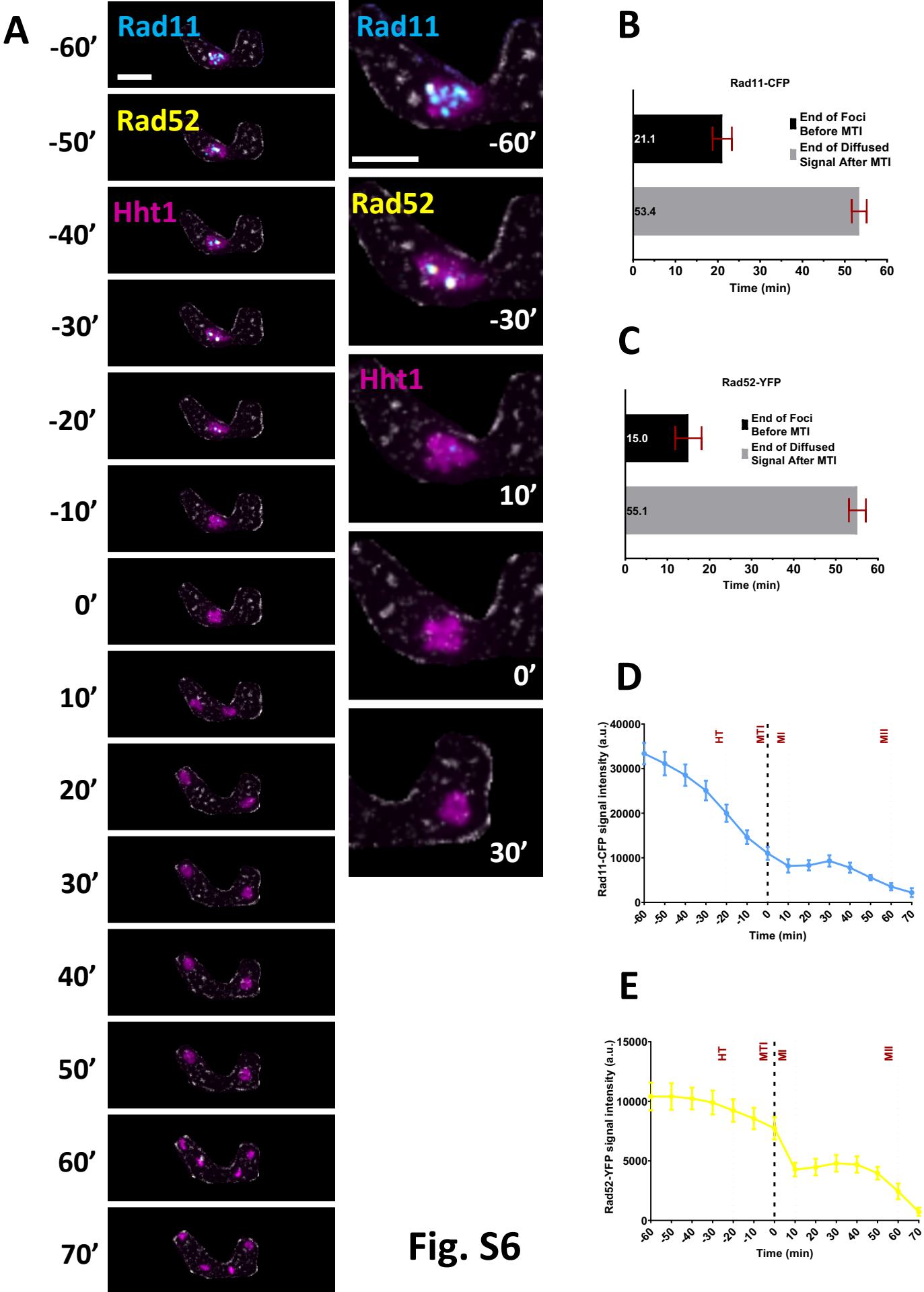
A
Rad11
Rad52
Hht1
-60'
-50'
-40'
-30'
-20'
-10'
0'
10'
20'
30'
40'
50'
60'
70'
Rad11
-60'
Rad52
-30'
Hht1
10'
0'
30'
B
Rad11-CFP
End of Foci Before MTI
End of Diffused Signal After MTI
21.1
53.4
0 10 20 30 40 50 60
Time (min)
C
Rad52-YFP
End of Foci Before MTI
End of Diffused Signal After MTI
15.0
55.1
0 10 20 30 40 50 60
Time (min)
D
Rad11-CFP signal intensity (a.u.)
0 10000 20000 30000 40000
HT
MTI
MI
MII
-60 -50 -40 -30 -20 -10 0 10 20 30 40 50 60 70
Time (min)
E
Rad52-YFP signal intensity (a.u.)
0 5000 10000 15000
HT
MTI
MI
MII
-60 -50 -40 -30 -20 -10 0 10 20 30 40 50 60 70
Time (min)

Fig. S6

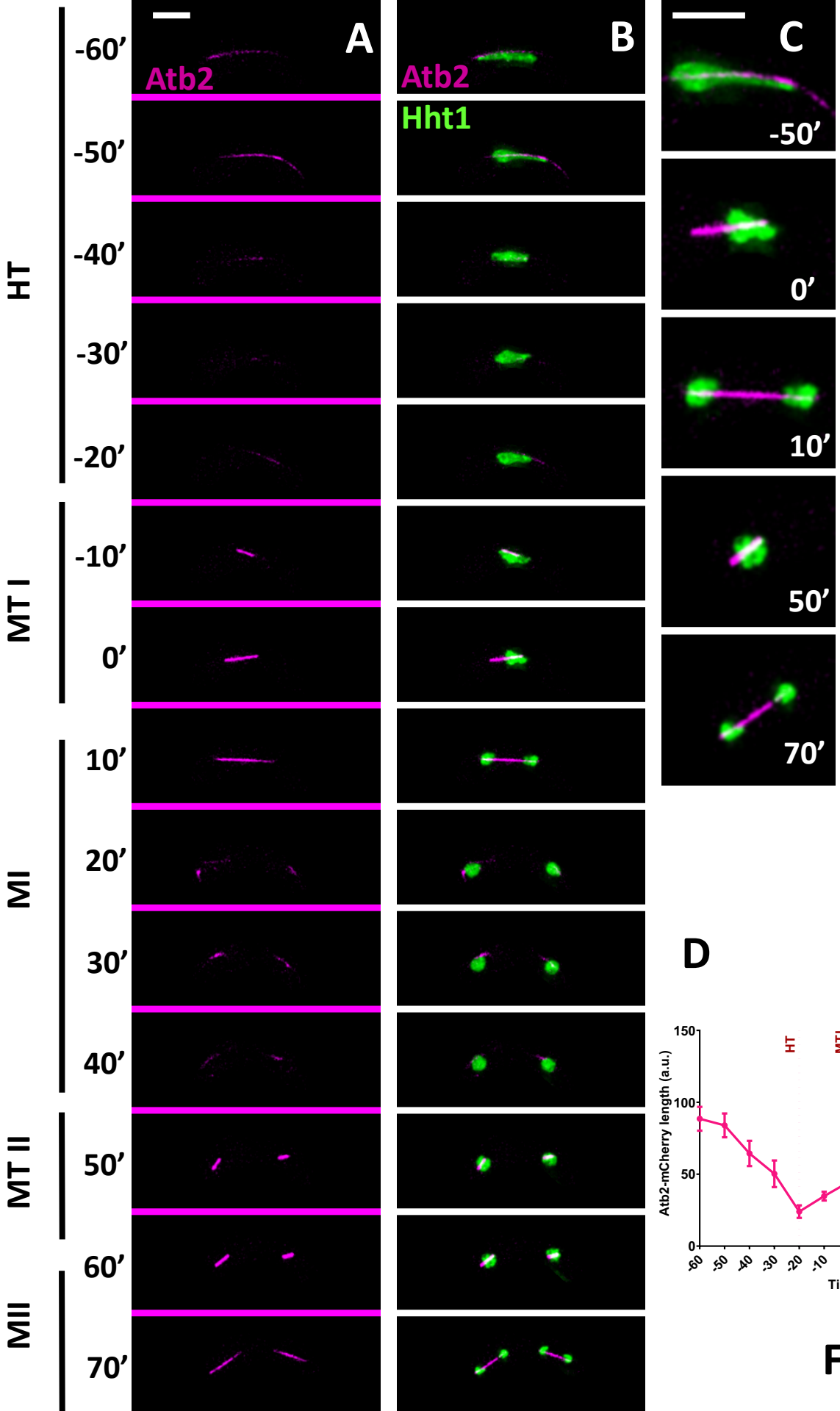
A
B
C
Atb2
Atb2
Hht1
HT
MT I
MI
MT II
MII
-60'
-50'
-40'
-30'
-20'
-10'
0'
10'
20'
30'
40'
50'
60'
70'
-50'
0'
10'
50'
70'

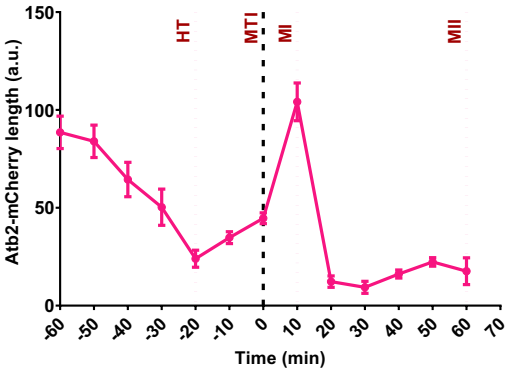
D
HT
MTI
MI
MII
Atb2-mCherry length (a.u.)
150
100
50
0
-60
-50
-40
-30
-20
-10
0
10
20
30
40
50
60
70
Time (min)

Fig. 6

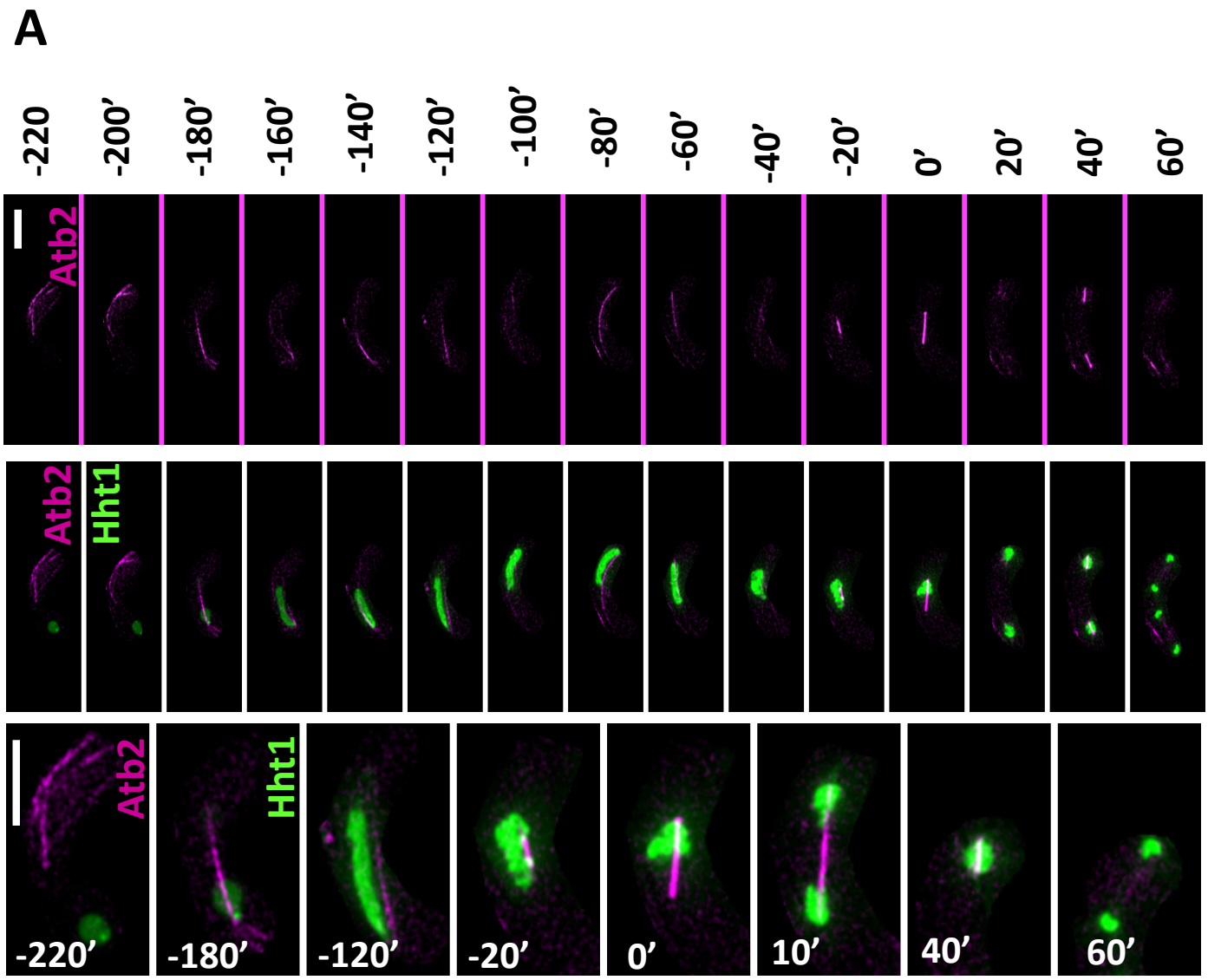
A
-220
-200'
-180'
-160'
-140'
-120'
-100'
-80'
-60'
-40'
-20'
0'
20'
40'
60'
Atb2
Atb2
Hht1
Atb2
Hht1
-220'
-180'
-120'
-20'
0'
10'
40'
60'

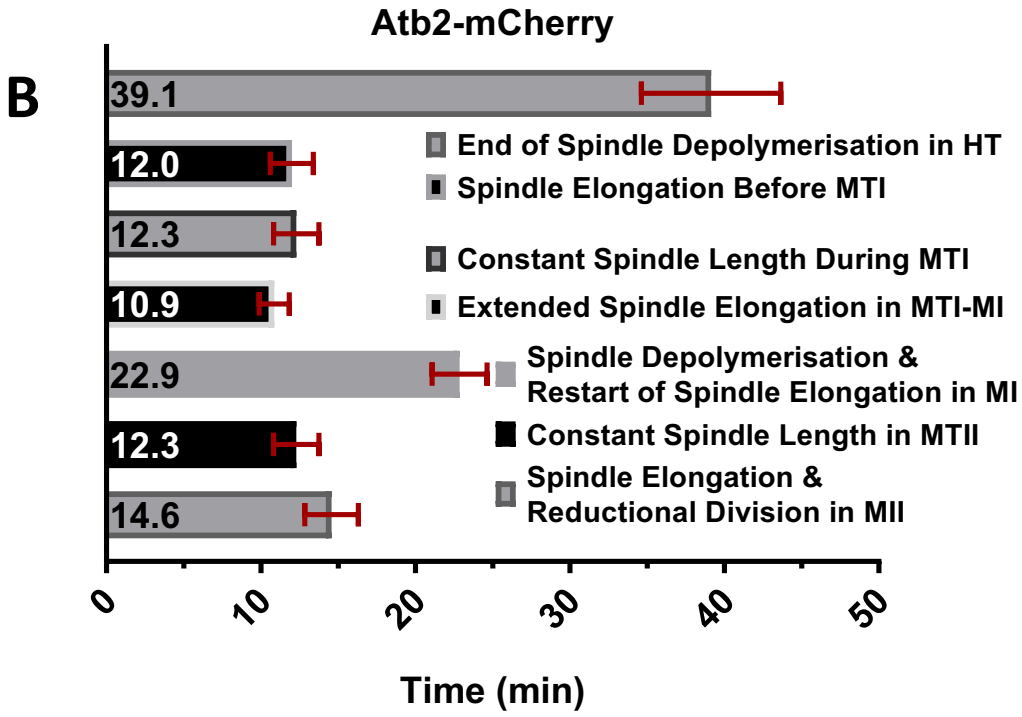
B
Atb2-mCherry
39.1
12.0
12.3
10.9
22.9
12.3
14.6
End of Spindle Depolymerisation in HT
Spindle Elongation Before MTI
Constant Spindle Length During MTI
Extended Spindle Elongation in MTI-MI
Spindle Depolymerisation &
Restart of Spindle Elongation in MI
Constant Spindle Length in MTII
Spindle Elongation &
Reductional Division in MII
0
10
20
30
40
50
Time (min)

Fig. S7

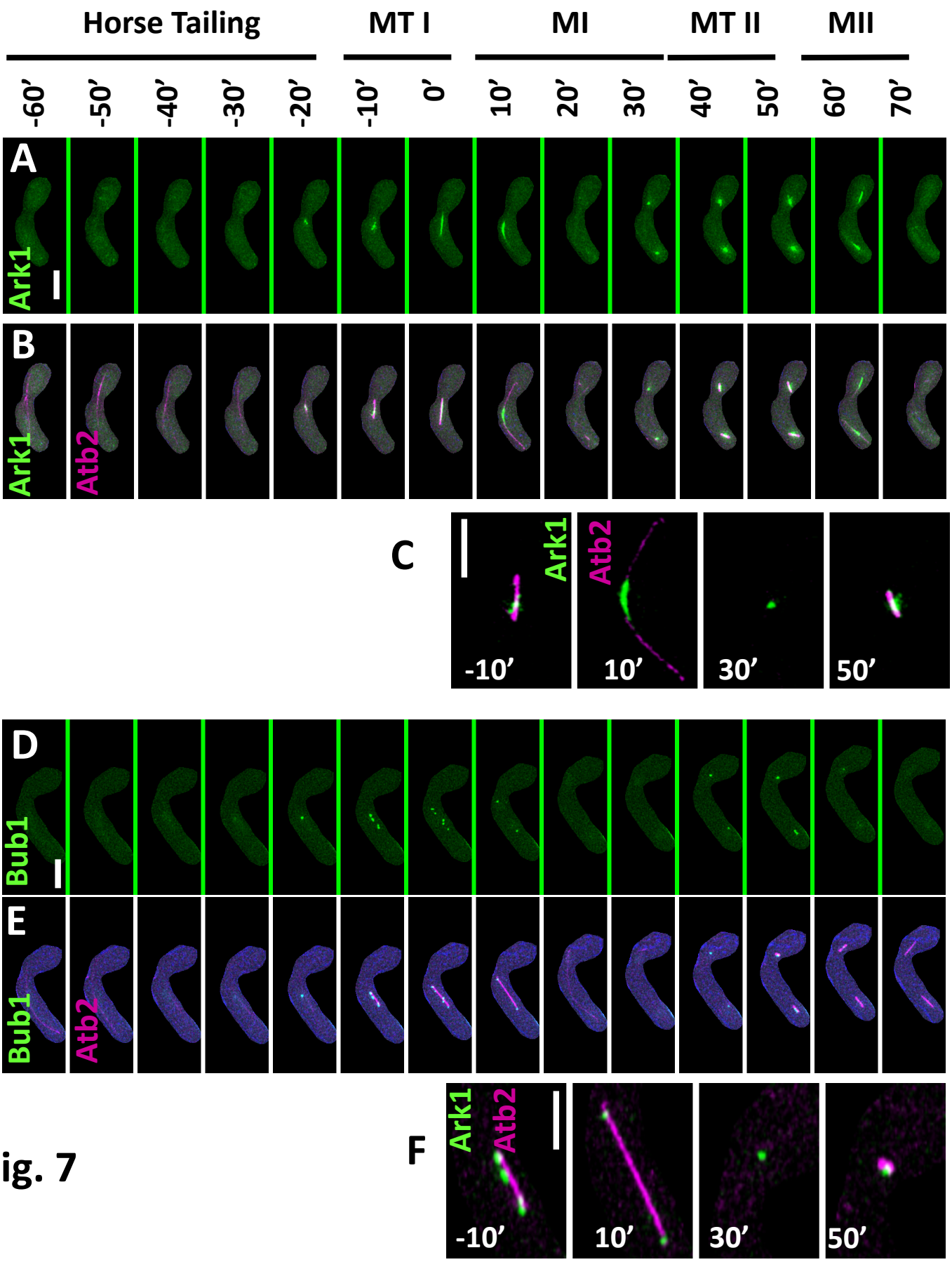
Horse Tailing
MT I
MI
MT II
MII
-60'
-50'
-40'
-30'
-20'
-10'
0'
10'
20'
30'
40'
50'
60'
70'
A
Ark1
B
Ark1
Atb2
C
Ark1
Atb2
-10'
10'
30'
50'
D
Bub1
E
Bub1
Atb2
F
Ark1
Atb2
-10'
10'
30'
50'

Fig. 7

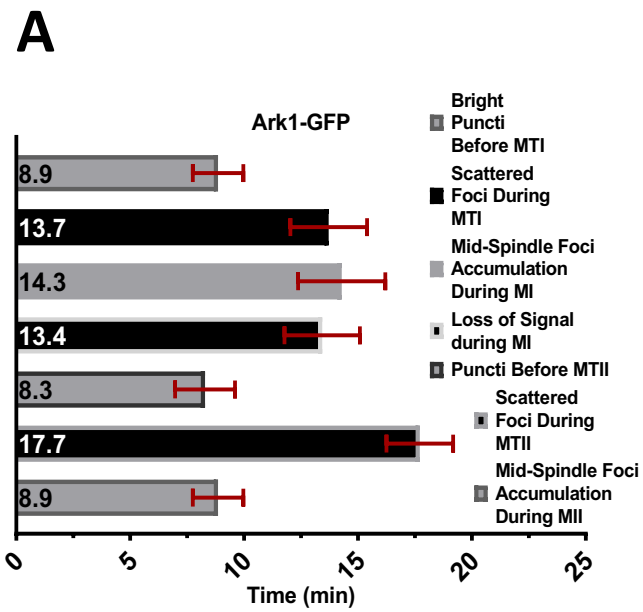
A
Ark1-GFP
Bright Puncti Before MTI
Scattered Foci During MTI
Mid-Spindle Foci Accumulation During MI
Loss of Signal during MI
Puncti Before MTII
Scattered Foci During MTII
Mid-Spindle Foci Accumulation During MII
8.9
13.7
14.3
13.4
8.3
17.7
8.9
0
5
10
15
20
25
Time (min)

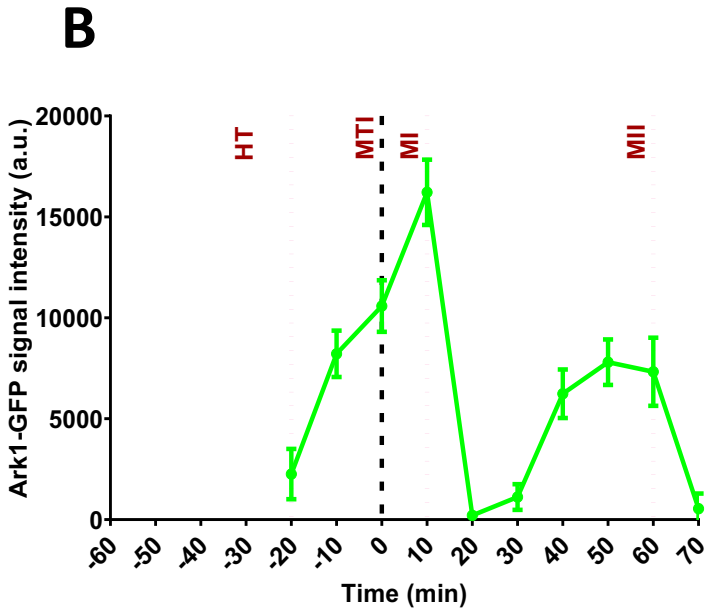
B
Ark1-GFP signal intensity (a.u.)
20000
15000
10000
5000
0
HT
MTI
MI
MII
-60
-50
-40
-30
-20
-10
0
10
20
30
40
50
60
70
Time (min)

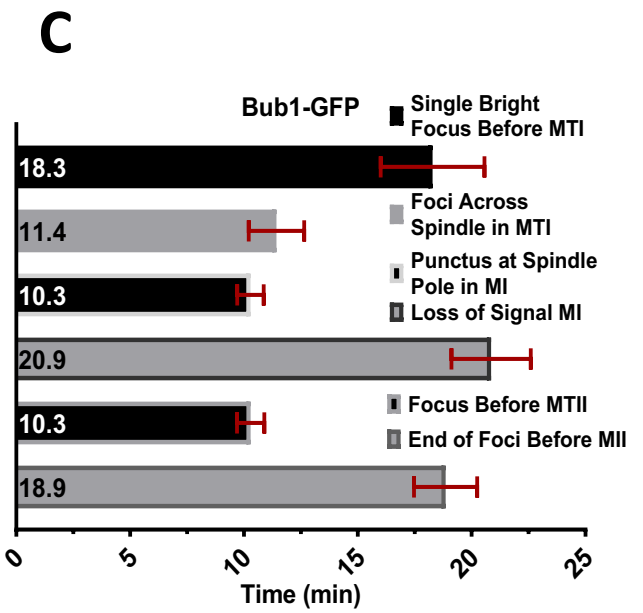
C
Bub1-GFP
Single Bright Focus Before MTI
Foci Across Spindle in MTI
Punctus at Spindle Pole in MI
Loss of Signal MI
Focus Before MTII
End of Foci Before MII
18.3
11.4
10.3
20.9
10.3
18.9
0
5
10
15
20
25
Time (min)

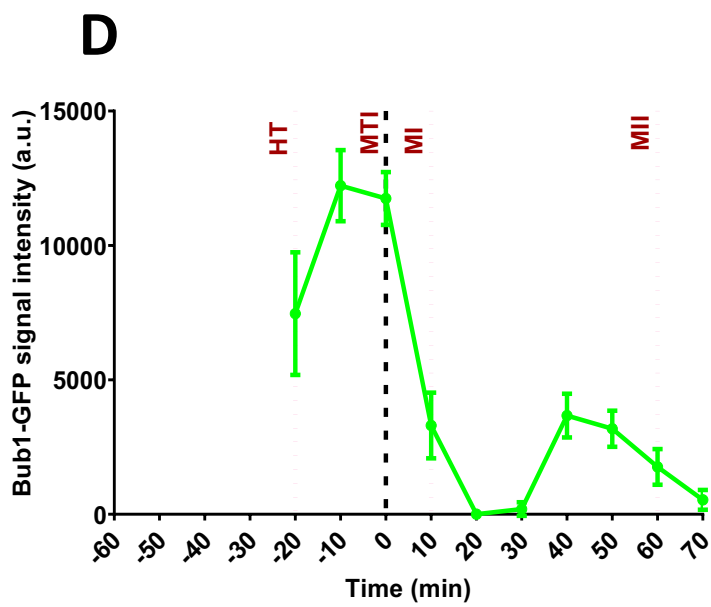
D
Bub1-GFP signal intensity (a.u.)
15000
10000
5000
0
HT
MTI
MI
MII
-60
-50
-40
-30
-20
-10
0
10
20
30
40
50
60
70
Time (min)

Fig S8

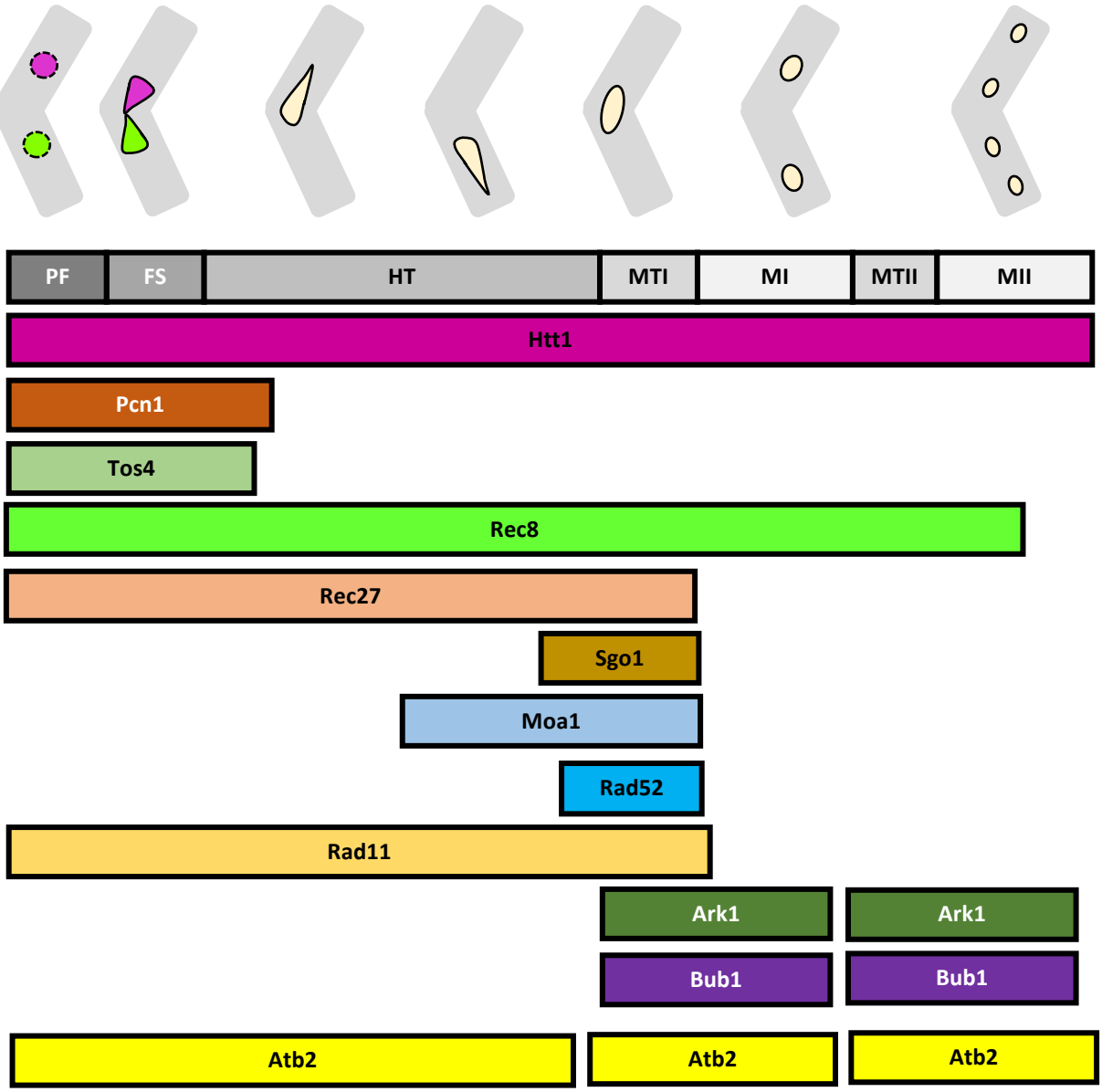
PF
FS
HT
MTI
MI
MTII
MII
Htt1
Pcn1
Tos4
Rec8
Rec27
Sgo1
Moa1
Rad52
Rad11
Ark1
Ark1
Bub1
Bub1
Atb2
Atb2
Atb2

Fig. 8

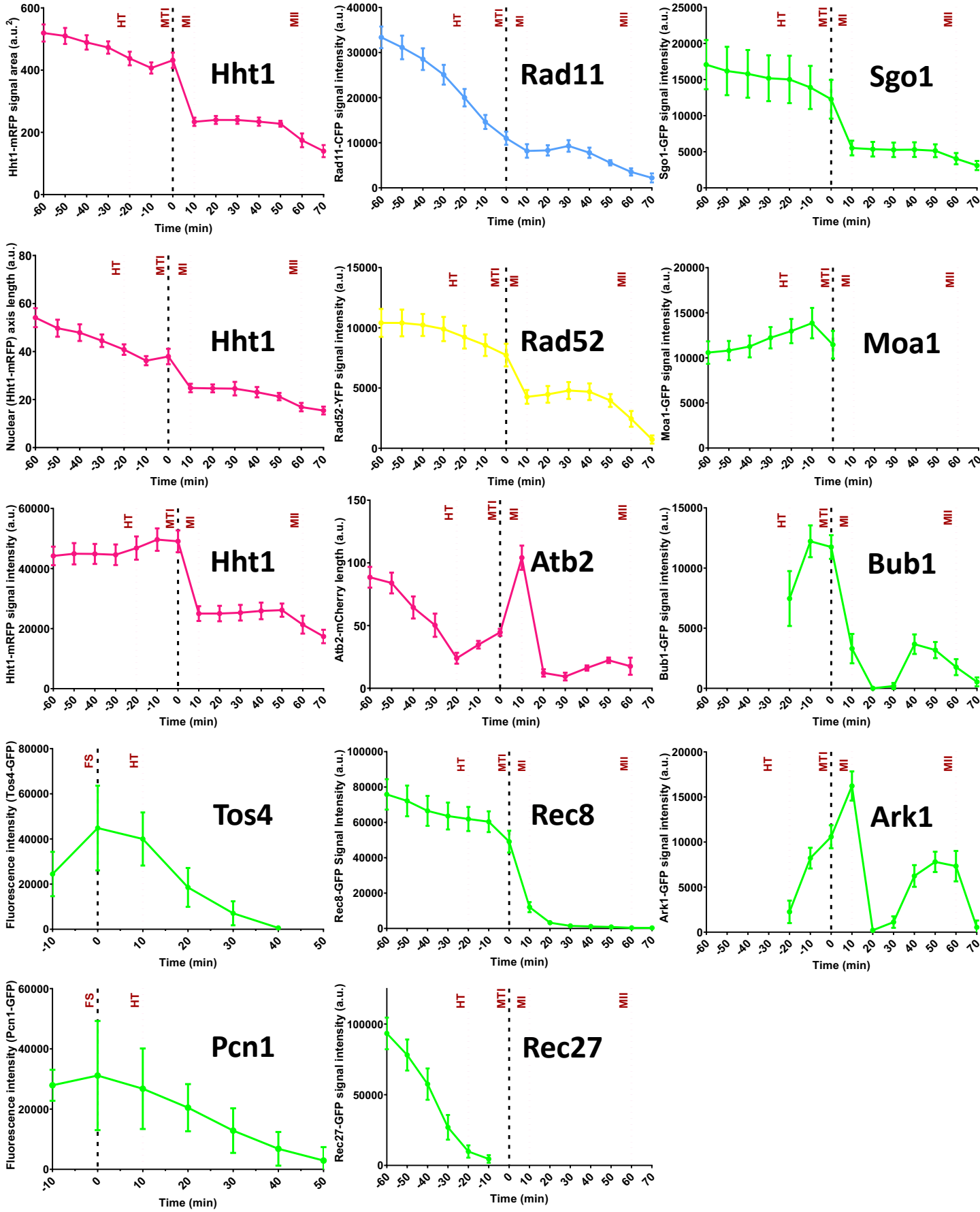
Hht1
Hht1-mRFP signal area (a.u.^{2})
Rad11
Rad11-CFP signal intensity (a.u.)
Sgo1
Sgo1-GFP signal intensity (a.u.)
Hht1
Nuclear (Hht1-mRFP) axis length (a.u.)
Rad52
Rad52-YFP signal intensity (a.u.)
Moa1
Moa1-GFP signal intensity (a.u.)
Hht1
Hht1-mRFP signal intensity (a.u.)
Atb2
Atb2-mCherry length (a.u.)
Bub1
Bub1-GFP signal intensity (a.u.)
Tos4
Fluorescence intensity (Tos4-GFP)
Rec8
Rec8-GFP Signal Intensity (a.u.)
Ark1
Ark1-GFP signal intensity (a.u.)
Pcn1
Fluorescence intensity (Pcn1-GFP)
Rec27
Rec27-GFP signal intensity (a.u.)
Time (min)
FS
HT
MTI
MI
MII

Fig. S9